NANODISCS FOR SPR ANALYSIS OF GPCR-G PROTEIN INTERACTIONS

PART II PROJECT 2014- 2015

WORD COUNT: 7688

G protein-coupled receptors (GPCRs) can mediate cascades of intracellular signalling by coupling to G proteins in response to activation by ligand. They are a highly significant group of membrane proteins in terms of their occurrence in mammalian genomes, the variety of downstream processes they mediate and their prominence and promise as drug targets. Details of how GPCRs and G proteins interact are therefore valuable from both pharmacological and biological points of view; however, the data available on these interactions is currently very limited.

A novel approach to assaying GPCR-G protein interactions has recently been developed, combining the advantages of Neurotensin receptor 1 (NTS1) as a model GPCR, nanodiscs for GPCR reconstitution, and SPR for real time, label free monitoring of protein-protein interactions. The aim of this project was to extend this SPR methodology to study the interaction of NTS1 with both a wild type and mutant version of the G protein $G\alpha_{i1}$.

Here, the necessary proteins were successfully expressed and purified, and avenues for increased yield of active NTS1 explored. NTS1-G protein interactions were assayed in a lipid environment shown to support improved ligand-binding activity for NTS1, and these interactions were shown to be sensitive to inverse agonism. In addition, areas in which the technique can be refined have been identified, which should facilitate further use of this methodology for studies of the GPCR-G protein interface.

TABLE OF ABBREVIATIONS

Abbreviation	**Meaning**
A_{280}	Absorbance at 280nm
BCA	Bicinchoninic acid
BPL	Brain polar lipid extract (Avanti)
cAMP	3'-5'-cyclic adenosine monophosphate
CD	Circular dichroism
CHS	Cholesteryl hemisuccinate
DDM	n-dodecyl-β-D-maltoside
DTT	Dithiothreitol
EDC	1-ethyl-3(3-dimethylaminopropal) carbodiimide hydrochloride
EDTA	Ethylenediaminetetraacetate
EL	Extracellular loop
GPCR	G protein-coupled receptor
GTP-γ-S	Guanosine 5'-*O*-(3-thiotriphosphate)
IL	Intracellular loop
IMAC	Immobilised metal ion affinity chromatography
IP_3	inositol 1,4,5-trisphosphate
K_D	Equilibrium dissociation constant
k_{off}	Dissociation rate constant
k_{on}	Association rate constant
MBP	Maltose binding protein
mP	Milli-polarisation units
MSP	Membrane scaffold protein

Mut	F336A G protein mutant
MWCO	Molecular weight cut off
NHS	N-hydroxysuccinimide
NT	Neurotensin
NT_{8-13}	Neurotensin residues 8-13
NTS1	Neurotensin receptor 1
NTS1B	N-MBP-TeV-rT43NTS1-his6 -TeV-TrxA-his10
OD_{600}	Optical density at 600nm
PA	Phosphatidic acid
PC	Phosphatidylcholine
PE	Phosphatidylethanolamine
PI	Phosphatidylinositol
POPC	(1-palmitoyl-2-oleoyl)-*sn*-glycero-3-phosphocholine
POPG	(1-palmitoyl-2-oleoyl)-sn-glycero-3-phospho-(1'-*rac*-glycerol)
PS	Phosphatidylserine
R_{max}	The SPR response when surface is saturated with analyte
SPR	Surface plasmon resonance
TeV	Tobacco etch virus protease
TM	Transmembrane
Tris	Tris(hydroxymethyl)aminomethane
TrxA	Thioredoxin

1. INTRODUCTION

1.1. G PROTEIN-COUPLED RECEPTORS

G protein-coupled receptors (GPCRs) constitute a protein superfamily that is the largest in mammalian genomes (Katritch *et al*, 2013). GPCRs can be sub-classified into one of five main families based on sequence similarity; rhodopsin (class A), secretin (class B), glutamate (class C), adhesion & frizzled/taste families (Fredriksson *et al*, 2003). Collectively, GPCRs bind a diversity of extracellular ligands including peptides, proteins, ions, hormones and neurotransmitters (Davies *et al*, 2007). Whilst the sequence identity between families is poor, and N terminal sequences vary considerably (Katritch *et al*, 2013), all GPCRs are unified by a 7-transmembrane (7TM) topology predictable from sequence. The class A receptors are by far the most numerous (~80% of GPCRs, (Davies *et al*, 2007) and are those for which the most structural information is available.

A number of features common to class A GPCRs are apparent from sequence, as well as a growing number of structures solved by X-ray crystallography (reviewed in (Katritch *et al*, 2013)) (figure 1).

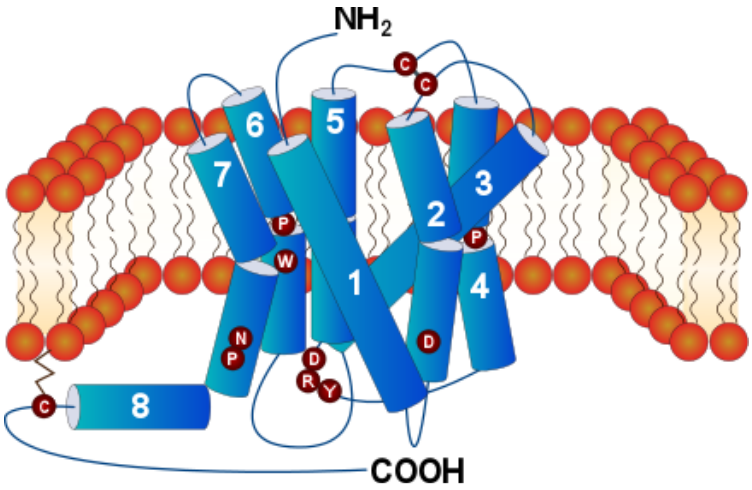

Figure 1: Common features of class A GPCRs. 7TM segments are connected by 3 extracellular and 3 intracellular loops (EL1,2,3 and IL1,2,3 respectively). Highly conserved amino acids are shown in red and include a disulfide bond between EL1 and EL2, prolines that help facilitate bends in TM helices and conserved motifs such as the DRY motif. Also shown are the extracellular amino-terminus, intracellular carboxy-terminus and amphipathic helix 8, which is in close proximity to a palmitoylated, semi-conserved cysteine. Adapted from (George *et al*, 2002).

A significant percentage of currently marketed drugs target a small fraction of GPCRs (36-50% of drugs, (Lagerström & Schiöth, 2008; Rask-Andersen *et al*, 2011)) and so GPCRs are of considerable pharmacological interest, especially when one considers that the majority of GPCRs are yet to be exploited as drug targets (>300) (Lagerström & Schiöth, 2008).

1.1.A) Mechanism of action

In brief, a GPCR is stimulated by a ligand, leading to conformational changes that facilitate G protein coupling; within the heterotrimeric Gαβγ assembly, GDP is exchanged for GTP in the Gα subunit, which dissociates from the Gβγ assembly (Pierce *et al*, 2002), facilitating downstream signalling (figure 2).

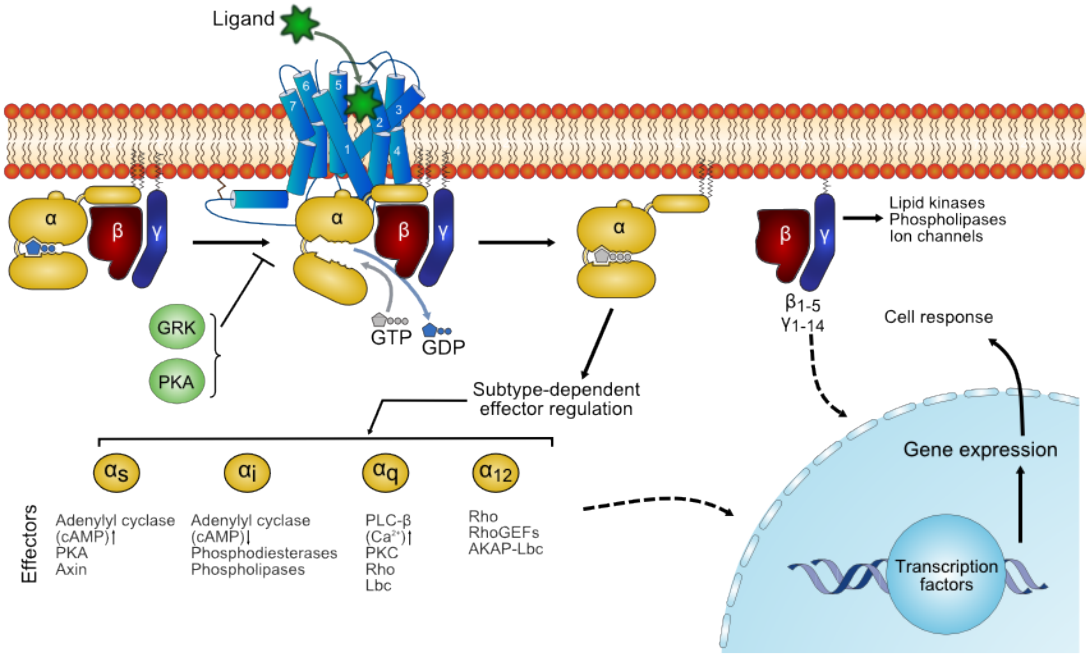

Figure 2: GPCR activation and signalling. Adapted from (Dorsam & Gutkind, 2007; George *et al*, 2002). *Both Gα and Gβγ are able to effect a range of downstream signalling processes, and complexity arises from the fact that a range of different Gα and Gβγ subunits exist, with the identity of the subunits determining signalling events downstream* (Dorsam & Gutkind, 2007). *Phosphorylation of the receptor by GRKs or PKA leads to binding of arrestins, which attenuate GPCR signalling and can facilitate GPCR internalisation (Ferguson, 2001). In addition, arrestins can facilitate G protein-independent GPCR signalling, by acting as scaffolds for additional signalling events* (Brzostowski & Kimmel, 2001). *PKA=protein kinase A, GRK=GPCR kinase, PLC-β =phospholipase C β, PKC=protein kinase C, GEF=guanine nucleotide exchange factor, AKAP-Lbc=A-kinase anchoring protein-Lbc.*

1.1.B) GPCR LIGANDS

GPCR ligands - both endogenous and exogenous - can be defined as agonists, inverse agonists and antagonists (figure 3).

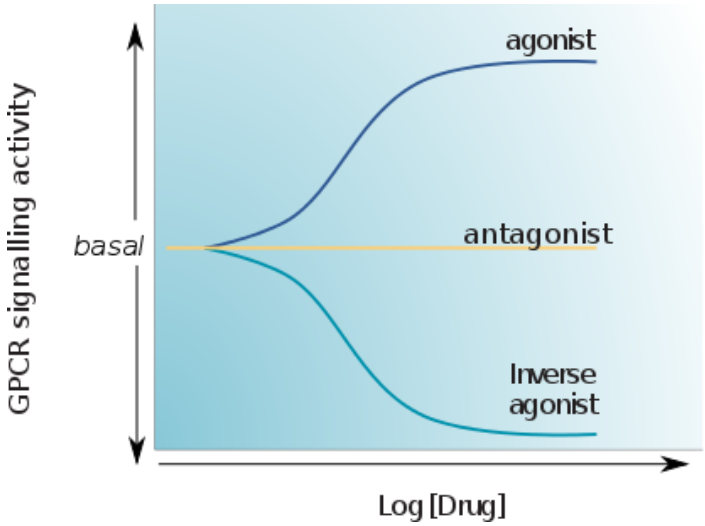

Figure 3: GPCR ligands. Agonists increase the proportion of receptor states capable of G protein activation beyond basal levels and inverse agonists decrease the proportion of these states below basal levels. Antagonists prevent the action of other ligands and do not themselves alter the number of active receptor states (Bartfai *et al*, 2004; Kenakin, 2004, 2009)*. Diagram adapted from* (Bartfai *et al*, 2004)*.*

Note, however, that many GPCR antagonists are likely to be inverse agonists, since inverse agonism is hard to detect with most pharmacological assays in GPCRs with low levels of basal activity (Kenakin, 2004; Barroso *et al*, 2002). Inverse agonism may be detected by using constitutively active GPCR mutants, or looking for effects of ligand on receptor conformation.

1.1.C) FEATURES OF THE ACTIVE STATE

GPCRs are proposed to exhibit a high degree of structural plasticity (Katritch *et al*, 2013; Manglik & Kobilka, 2014). Analysis of a variety of class A GPCR crystal structures reveals unifying features for the signalling-active state of these receptors, namely rearrangements of TM helices on the intracellular side of the receptor, in particular an outwards movement of helix VI and corresponding movement of helix V (Katritch *et al*, 2013).

1.2. GPCR-G PROTEIN INTERACTIONS

1.2.A) STRUCTURAL BASIS

Structural information for GPCR-G protein interactions comes mainly from a crystal structure of a complex of the agonist-bound β_2-adrenergic receptor (β2AR) and nucleotide free G_s-heterotrimer (Rasmussen *et al*, 2011). This

represents an active transmembrane-signalling complex. Gβ and Gγ make no direct contacts to the receptor, although they do influence the receptor-G protein interaction (Chung *et al*, 2011). Many of the interactions are centred around the insertion of the C terminal α5-helix of Gα into a pocket on the GPCR created by movement of helix VI (figure 4). Of the 21 G_s amino acids within 4Å of the receptor, only 5 are conserved with G_i, and all of these are in α5.

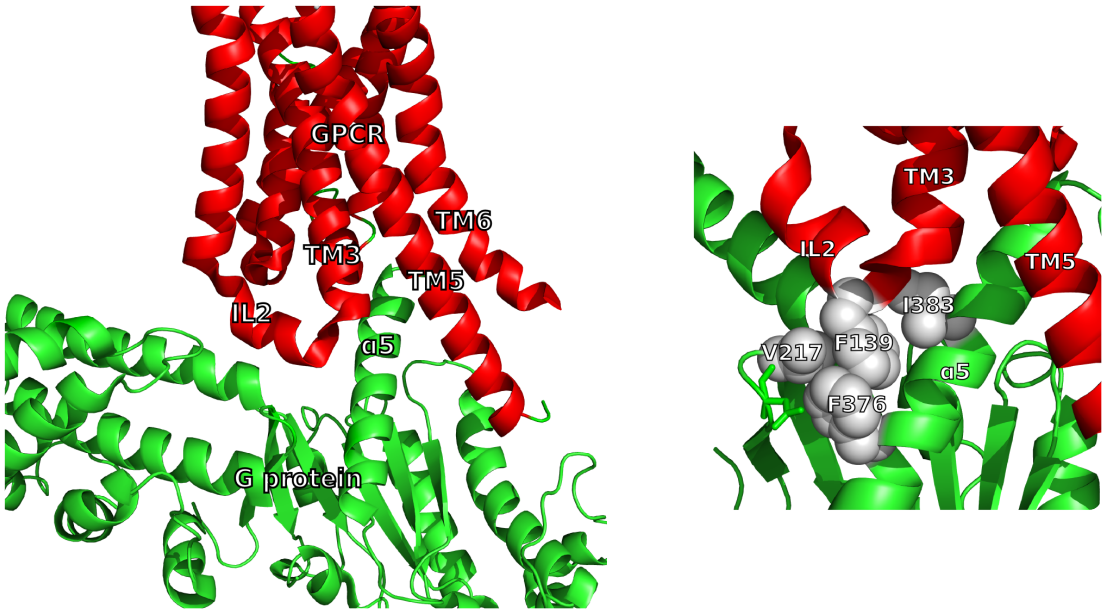

Figure 4: Structural basis of β2AR-G_s interactions. Left: Overview of the GPCR-G protein interface, showing insertion of the α5 helix on G_s into a cleft formed in the activated GPCR. Right: A hydrophobic network centred around a F139 of IL2 on the receptor, including a π-stacking interaction with F376. Image produced in pymol from the structure published by (Rasmussen *et al*, 2011), *PDB ID: 3SN6.*

1.2.B) Quantifying GPCR-G protein interactions

There is a relative paucity of information on the thermodynamics and kinetics of GPCR-G protein interactions. In many cases, G protein coupling is assayed for by a radioligand-binding assay using GTP-γ-^{35}S; this is a non-hydrolysable analogue of GTP and in the presence of an active GPCR, the G protein will exchange bound GDP for GTP-γ-^{35}S (Pelaprat, 2006; Leitz *et al*, 2006; Inagaki *et al*, 2012). This experiment is simple, but does not directly assay the GPCR-G protein interface. Some indication comes from experiments using plasmon-waveguide resonance spectroscopy, which has been used to quantify interactions between μ-opioid receptors and different G proteins, in different ligand-bound states of the receptor (Alves *et al*, 2003) (table 1).

Bound ligand	Apo	Agonist	Antagonist
Approximate K_D for GPCR-G protein interaction (nM)	60	10	500

Table 1: Plasmon-waveguide resonance spectroscopy of GPCR-G protein interactions. Shown are data for the μ-opioid receptor interaction with a G protein mixture containing $G\alpha_o/_{i1}/_{i2}/_{i3}$ + Gβγ, and its dependence on the ligand-bound state of the receptor. Based on a table in (Alves *et al*, 2003).

1.3. Reconstitution of GPCRs

Whilst GPCRs can be studied in the context of the cell or in cell preparations, for most biophysical studies the receptor is first extracted from membranes and solubilised using detergent, then purified (Grisshammer, 2009; Serebryany *et al*, 2012). However, detergent-GPCR complexes are not an ideal form in which to study GPCRs. Firstly, many GPCRs show poor stability in detergent solution, likely as a result of the structural plasticity described (Jaakola *et al*, 2008; Grisshammer, 2009). Secondly, processes including ligand binding and G protein binding show sensitivity to lipid composition (Inagaki *et al*, 2012; Oates *et al*, 2012) and in some GPCR crystal structures lipids are observed to remain after detergent solubilisation suggesting functional significance (e.g. (Jaakola *et al*, 2008)).

A solution to this issue is to reconstitute pure, detergent-solubilised receptor into a membrane-like environment such as a liposome or nanodisc. An overview of detergents, liposomes and nanodiscs for the study of GPCRs is given in figure 5.

1.3.A) Nanodiscs

Nanodiscs are a relatively recent technology for the reconstitution of membrane proteins, developed by Sligar and co-workers. Membrane scaffold protein (MSP) consists of several amphipathic helices, defining the perimeter of the bilayer - different length MSP constructs are available which define nanodiscs of different diameters (Denisov *et al*, 2004; Ritchie *et al*, 2009). The result is a particle of greater stability and size homogeneity than liposomes (Borch *et al*, 2008); they are amenable to many techniques and treatments one would apply to a soluble protein, such as chromatography and bulk spectroscopic techniques (Bayburt & Sligar, 2010; Serebryany *et al*, 2012) . Moreover, proteins can be reconstituted into nanodiscs with defined oligomeric state (a factor that is difficult to control for liposomes) and using, in theory, any bilayer-forming lipids (Bayburt & Sligar, 2010).

Unlike in liposomes, for proteins in nanodiscs there is simultaneous access of aqueous solution to either side of the bilayer/reconstituted protein (Serebryany *et al*, 2012).

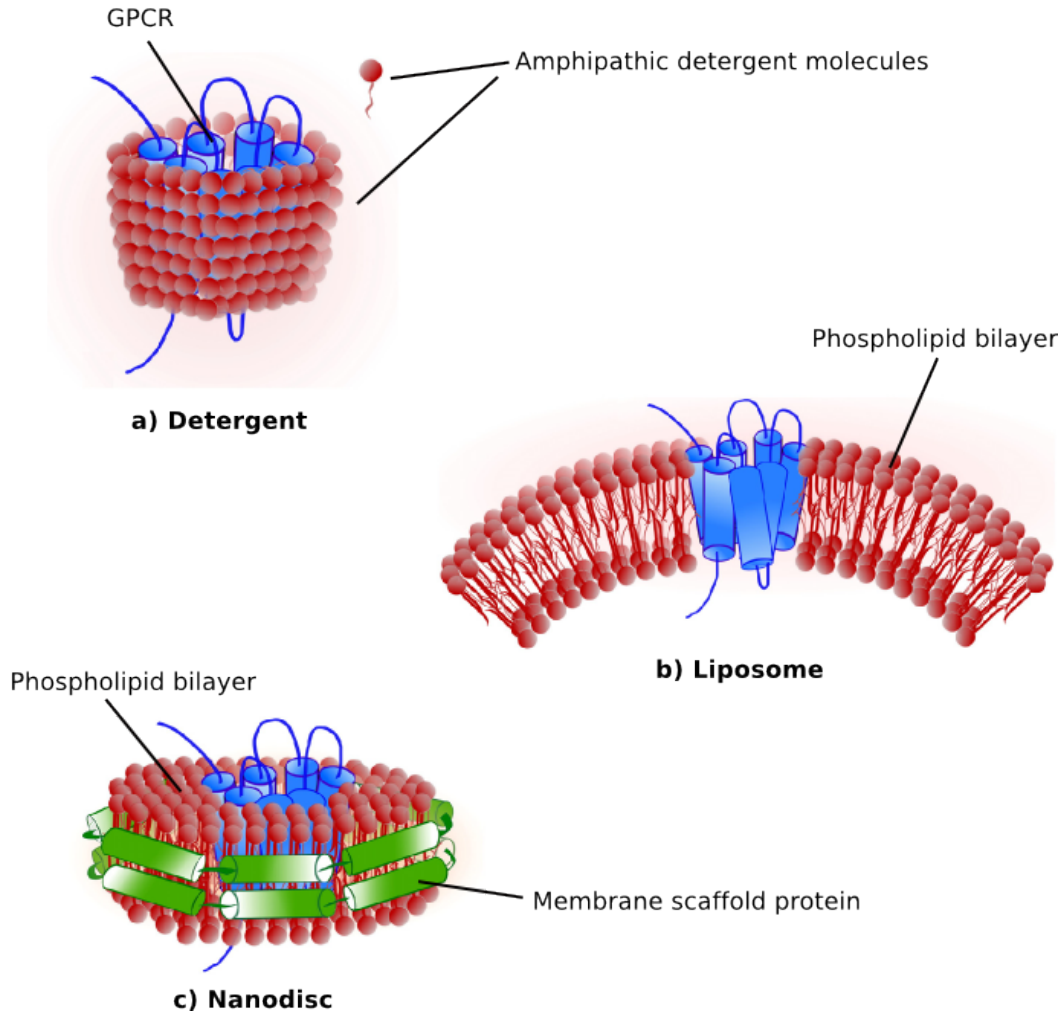

Figure 5: A GPCR in three different environments. Adapted from (Serebryany *et al*, 2012)*. A) A detergent-GPCR complex where the hydrophobic tails of the detergent assemble around transmembrane regions of the protein, whilst hydrophilic moieties face aqueous solution* (Le Maire *et al*, 2000)*. B) Liposome; shown is a unilamellar phospholipid vesicle, although multi-lamellar liposomes can be made. Liposomes are a sealed phospholipid bilayer with an aqueous inner compartment, with potential diameters ranging from 0.025 to 250 μm* (Jesorka & Orwar, 2008)*. C) A nanodisc; a lipid bilayer encircled by 2 copies of membrane scaffold protein (MSP)* (Denisov *et al*, 2004).

Several GPCRs have now been reconstituted into nanodiscs For example, β_2-adrenergic receptor (β_2-AR) (Leitz *et al*, 2006), was reconstituted and shown to bind various ligands and couple to G protein - events which occur on opposite sides of the membrane but which can both be studied using nanodiscs. Rhodopsin (Ritchie *et al*, 2009), CCR5 (Knepp *et al*, 2011) and NTS1 (Adamson & Watts, 2014) have also been reconstituted into nanodiscs, generally in a form capable of ligand and/or G protein-binding.

1.4. Surface Plasmon Resonance

Surface plasmon resonance (SPR) is a biophysical method that is commonly used in analysis of both affinities and association/dissociation kinetics of protein-ligand/protein-protein interactions, reviewed in (Jason-Moller *et al*, 2006). The method uses a gold-coated biosensor chip that forms the floor of microfluidic flow cell. One of the interaction partners is immobilised on the chip surface (the *ligand*), whilst the other is injected into the flow cell at a range of concentrations (the *analyte*).

In SPR, interactions are detected through changes in refractive index that occur within 300nm of the surface of the gold film as a result of analyte-ligand interactions. The change in refractive index is reported in response units (RU) directly proportional to the mass of protein in this surface layer (i.e. bound to surface). Hence SPR allows interactions to be monitored in real-time without labels with a high degree of sensitivity (Jason-Moller *et al*, 2006; Patching, 2014; Glück *et al*, 2011). A summary of a simple SPR experiment and sensorgram is shown in figure 6.

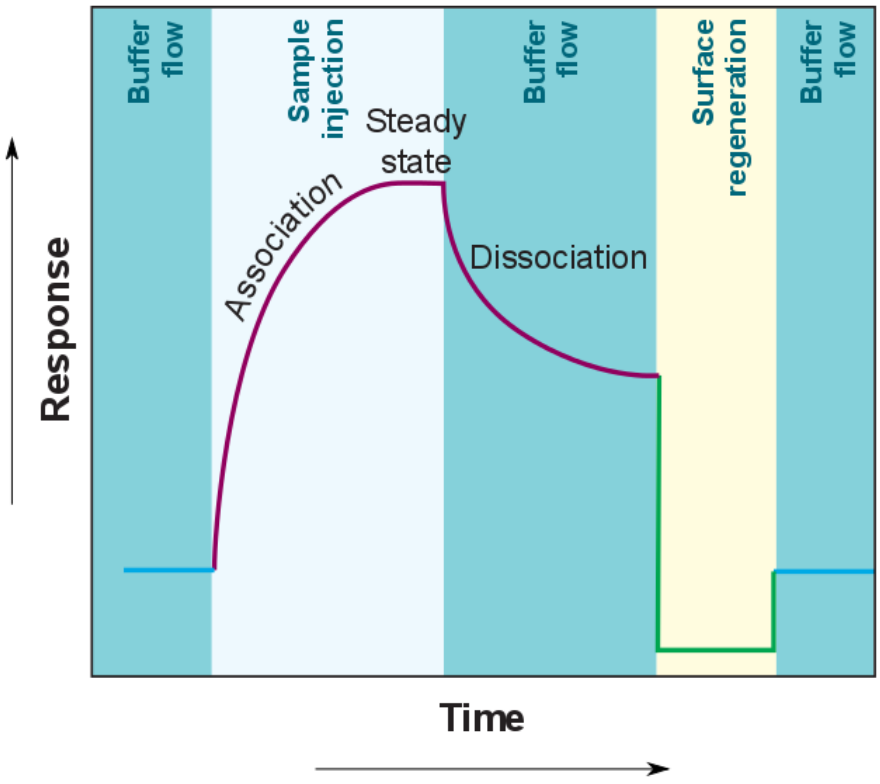

Figure 6: A simple sensorgram and SPR experiment. After establishment of a baseline, sample is injected and the analyte associates with the ligand on the chip surface, before reaching a steady state where there is no net loss or gain of material at the chip surface. Flow of buffer then initiates dissociation of bound

analyte from the surface, which is then regenerated for a further experiment. Figure adapted from (Wilson, 2002).

1.4.A) SPR STUDIES OF MEMBRANE PROTEINS

In addition to being used to study interactions between immobilised ligand and detergent-solubilised membrane protein, several SPR methodologies have been developed for studying membrane proteins in a more native-like environment (reviewed in (Patching, 2014)). These include use of an L1 chip (Biacore), the surface of which is functionalised with lipophilic moieties; this has been used to capture proteoliposomes and facilitate on-chip reconstitution of detergent-solubilised GPCRs into bilayer-like structures (Stenlund *et al*, 2003). However, a major disadvantage of such techniques is that only one face of the membrane is exposed to solution, meaning certain binding sites may be made unavailable to the analyte. This is especially a problem when one considers that in such systems there may be heterogeneity in the orientation of the protein within the bilayer (Borch *et al*, 2008). A recent development has been the use of nanodiscs as an analyte in SPR (Glück *et al*, 2011; Adamson & Watts, 2014), which can overcome such potential problems.

1.5. NEUROTENSIN RECEPTOR 1

Neurotensin receptor 1 (NTS1) is a class A GPCR expressed in the brain and intestine (Vincent et al., 1999) and named for its ligand, neurotensin (NT). This 13 amino acid peptide (ELYENKPRRPYIL) binds to NTS1 with nanomolar affinity (Tucker,J. & Grisshammer,R., 1996; Vincent *et al*, 1999; Vita *et al*, 1993). Residues 8-13 of NT (NT_{8-13}) confer all the biological activity of NT ((Kitabgi *et al*, 1977) and this binding is inhibited by Na^+ and GTP (Kitabgi, 2006). NT is found in the central nervous system, where it acts as a neurotransmitter, and in the gastrointestinal tract, where it acts as a local hormone. It has been implicated in a diversity of physiological processes including hypothermia, modulation of dopamine signalling and gastric acid secretion (reviewed in (Dobner, 2005; Mustain *et al*, 2011; Vincent *et al*, 1999)). Moreover, it is implicated in the pathogenesis of conditions including schizophrenia, intestinal inflammation and a variety of cancers. Importantly, whilst other neurotensin receptors exist, NTS1 is believed to mediate most of the physiological roles and pharmacological effects of NT (Dobner, 2005). Hence NTS1 is both of significant biological interest and considerable pharmacological potential, even amongst other GPCRs.

NTS1 coupling to G_q, G_s and G_i subtypes of the G_α subunit has been observed (Kitabgi, 2006), as has beta-arrestin dependent internalisation (Oakley *et al*, 2001). NTS1 ligands include the endogenous ligand NT and SR48692, a non-peptide ligand developed by Sanofi-Aventis. This has been described as an antagonist and has an IC_{50} of 32nM (Vita *et al*, 1993; Kitabgi, 2006).

Moreover, whilst expression of membrane proteins is often problematic in terms of obtaining sufficient amounts of active protein (Bernaudat *et al*, 2011), protocols exist for expression of functional NTS1 in *E. coli* in milligram amounts (Grisshammer *et al*, 2005) (figure 7).

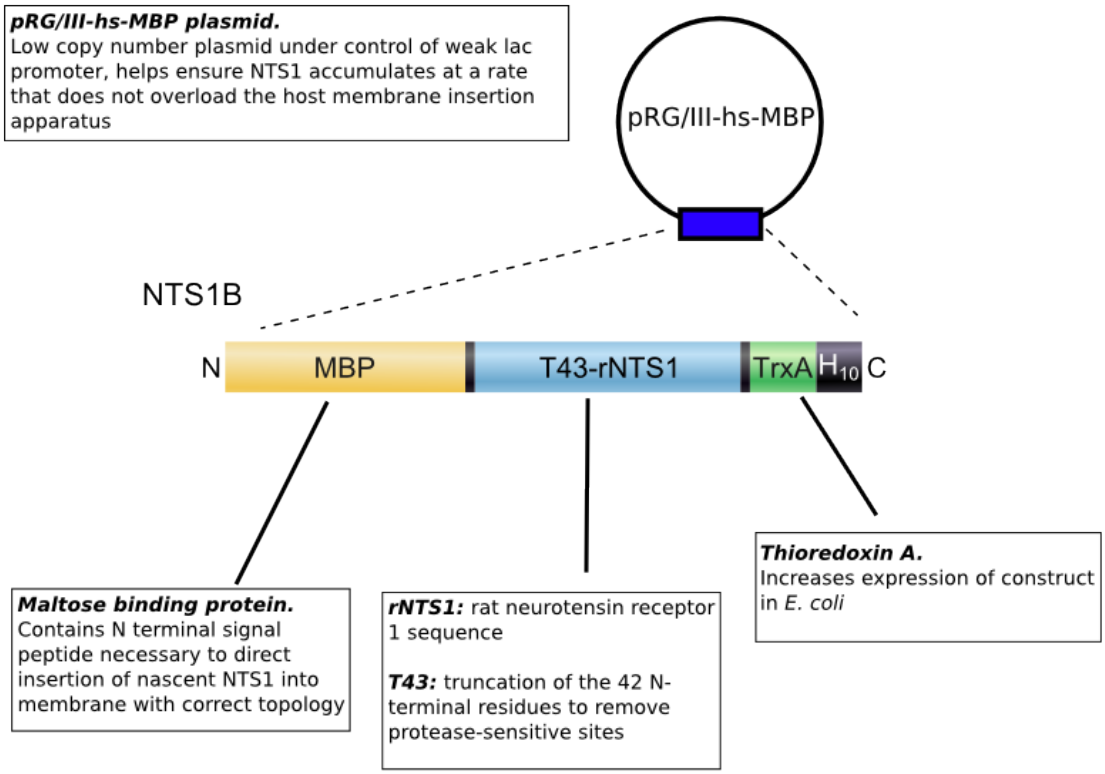

Figure 7: Features of the NTS1 expression system. Based on figures and information in (Tucker & Grisshammer, 1996; Grisshammer *et al*, 2005)*. The sequence used is Rat NTS1, which shares 84% amino acid identity and 92% similarity with human NTS1 (Vita et al., 1993) and so is likely to model human NTS1 well.*

Several crystal structures for NTS1 exist, for example ID 4GRV (White *et al*, 2012) and PDB ID 3ZEV (Egloff *et al*, 2014b). Hence in addition to its interest from a biological and pharmacological perspective, NTS1 is a tractable GPCR experimentally; it can be expressed in a simple host system and has structural information available for interpretation of results at the molecular level.

1.5.A) NTS1-G PROTEIN INTERACTIONS

Expression of mutant NTS1 receptors in Chinese hamster ovary cells has established that NTS1-IL3 sequences are required for G_q activation, whilst the C-terminal domain is required for G_s and G_i activation by the receptor (Kitabgi, 2006). Curiously, an F358A mutation in TM7 gives constitutive activation of inositol 1,4,5-trisphosphate (IP_3) production (G_q) but not 3'-5'-cyclic adenosine monophosphate (cAMP) production (G_s). NT acts as an agonist on this mutant,

increasing both IP_3 and cAMP production. SR46892 is found to act as an inverse agonist, which decreases IP_3 production below the constitutively active level.

There is also some evidence for a role of lipids in differential coupling of NTS1 to G protein subtypes. G_q coupling to NTS1 shows lipid-dependent affinity; levels of bound GTP-γ-^{35}S increase with increasing POPG content (Inagaki *et al*, 2012). However, for the G_i subtype, affinity for NTS1 measured by microscale-thermophoresis was observed to increase with increasing content of brain polar lipids (BPL, Avanti) in the lipid environment of NTS1 (P. Dijkman & A. Watts, in preparation). The content of BPL is shown in table 2.

Component species	Weight of component/total weight of extract (%)
PC	12.6
PE	33.1
PI	4.1
PS	18.5
PA	0.8
Unknown	30.9

Table 2: Lipid composition of the brain polar lipid extract supplied by Avanti. This represents the acetone-soluble fraction of total porcine brain lipids. PC, PE, PI, PS, PA= phosphatidylcholine, phosphatidylethanolamine, phosphatidylinositol, phosphatidylserine, phosphatidic acid respectively. Table reproduced from http://www.avantilipids.com

Interestingly, NT-binding is also highest in BPL (Oates *et al*, 2012), and PE content appears to be significant: BPL liposomes support highest activity, followed by a PE-PC mix, then pure PC liposomes.

1.5.B) Quantifying NTS1-G protein interactions; work from the host laboratory

The host laboratory has developed an SPR protocol for studying interactions between NTS1-nanodiscs and G proteins (Adamson & Watts, 2014). The highest quality results have been obtained with NTS1-nanodiscs as analytes and the G protein immobilised by amine coupling (figure 8). The results obtained in these experiments are summarised in figure 9 and table 3.

For each condition, two sets of parameters are reported, since the data is fitted using a heterogeneous ligand-binding model. This assumes that there are two distinct, independent binding events between analyte and ligand. This gives the fit more degrees of freedom, so it is generally of higher quality than for a simple 1:1 analyte:ligand binding model. The use of the fit is likely justified here since amine-coupling gives rise to heterogeneity in orientation of the ligand on the chip surface when multiple amines are available. Analysis of a $G\alpha_{i1}$ crystal

structure (PDB ID: 2G83, (Johnston *et al*, 2006)) reveals that many of the 27 lysines present are surface exposed and are distributed across the entire surface, including areas known to bind to GPCRs.

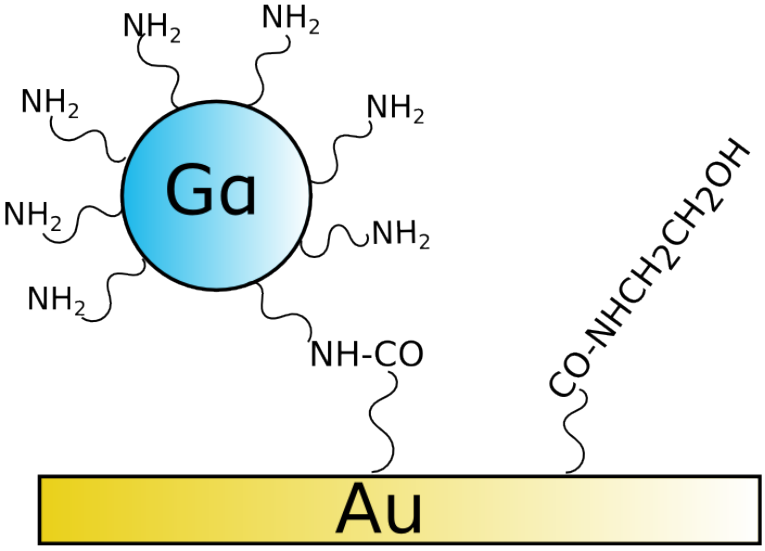

Figure 8: G protein amine coupling to an SPR chip surface (Au). G protein is captured by formation of an amide bond (NH-CO) between a G protein amine groups and carboxylated dextrans on the chip surface, facilitated by use of the reagents EDC (1-ethyl-3(3-dimethylaminopropal) carbodiimide hydrochloride) and NHS (N-hydroxysuccinimide) in a 1:1 mixture. Following the ligand capture, any remaining carboxylates are blocked with ethanolamine ($NH_2CH_2CH_2OH$). Due to the presence of many amine groups of the surface of the G protein, there is likely to be heterogeneity in the orientation of immobilised G protein on the surface.

The K_D values are of similar magnitude to those discussed for the μ-opioid receptor (table 1) and experiments using G protein as the analyte with nanodiscs immobilised on an L1 chip give parameters that are not significantly different to those presented (Adamson & Watts, 2014).

The method described is thus a promising avenue for quantifying GPCR-G protein interactions by directly assaying the GPCR-G protein interface. The use of nanodiscs means the system should be amenable to the study of GPCR-G protein interactions in the presence and absence of different ligands, and different lipid environments. The discussed results come from NTS1 reconstituted into 1-palmitoyl-2-oleoyl)-sn-glycero-3-phospho-(1'-*rac*-glycerol) - 1-palmitoyl-2-oleoyl)-sn-glycero-3-phosphocholine (POPC-POPG) nanodiscs, which form readily but which may be sub-optimal for certain NTS1 activities as discussed. These results also consider only NT-bound NTS1; given the results discussed in section 1.5.A), it would be interesting to assay the interactions in a more native-like lipid environment and under different ligand-bound states of NTS1.

In addition, Roslin Adamson has produced a plasmid with a $G\alpha_{i1}$ sequence containing an F336A mutation. F336 aligns with F376 of G_s (figure 4). Rat-NTS1 possesses a phenylalanine in IL2, F175, which aligns with F139 of β2AR. Hence there are equivalent residues on NTS1 and $G\alpha_{i1}$ to make the interaction shown in figure 4B; if the F336A sequence can be expressed and purified, the mutant protein can be used to test for the contribution of F336 to the NTS1-$G\alpha_{i1}$ interface, and so to analyse conservation of interactions at this interface with the β2AR-Gs interface.

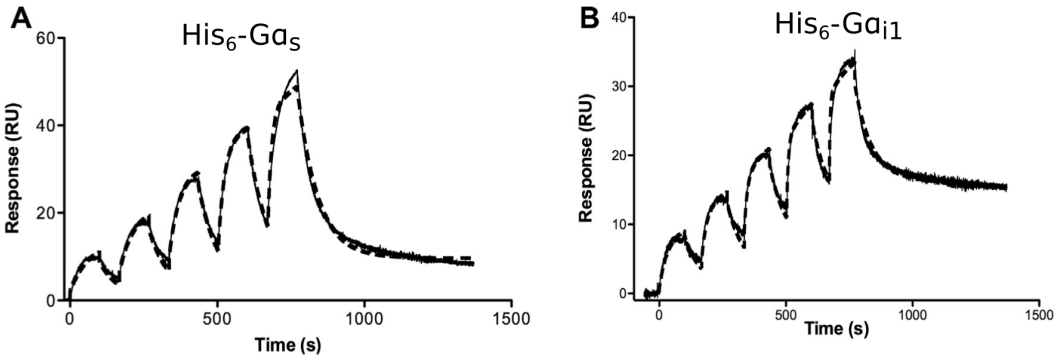

Figure 9: NTS1-Gα interactions. Sensorgrams obtained for interaction of NTS1 with A) $G\alpha_s$ and B) $G\alpha_{i1}$, showing both the measured response (black line) and fitted response (dotted line) derived from a heterogeneous ligand fit. The data was collected in single-cycle kinetics mode, whereby analyte is injected at increasing concentrations without regeneration steps in-between (compare to figure 6). Figure reproduced from (Adamson & Watts, 2014).

Parameter	Value	SE	N	Value	SE	N
k_{a1} ($M^{-1}s^{-1}$)	1.9×10^5	1.9×10^3	12	3.2×10^5	340	6
k_{d1} (s^{-1})	2.4×10^{-3}	4.2×10^{-5}	12	1.1×10^{-2}	8.4×10^{-6}	6
K_D1 (nM)	31	18	12	15	6	6
$R_{max}1$ (RU)	29	16	12	29	15	6
k_a2 ($M^{-1}s^{-1}$)	4.6×10^5	3.0×10^4	10	1.4×10^5	2.8×10^3	6
k_d2 (s^{-1})	4.4×10^{-1}	7.5×10^{-3}	10	1.6×10^{-2}	1.1×10^{-4}	6
K_D2 (nM)	470	130	10	330	170	6
R_{max} 2 (RU)	33	10	10	37	15	6

Table 3: Parameters derived from the fitted response shown in figure 9. SE = standard error determined from replicate experiments. N= number of replicate experiments. Table reproduced from (Adamson & Watts, 2014).

1.6. AIMS OF THE DISSERTATION

The aims of this dissertation are to:

1. Express and purify NTS1 in sufficient quantity for reconstitution of NTS1 into nanodiscs made from brain polar lipids. This also requires expression and purification of MSP and Tobacco etch virus protease (TeV);
2. Express and purify the $G\alpha_{i1}$ F336A mutant;
3. Use SPR to characterise the interactions between NTS1 in BPL-nanodiscs and both wild type and F336A $G\alpha_{i1}$;
4. Use SPR to analyse the effect of the absence of any ligand (Apo-receptor), the presence of NT_{8-13} and the presence of SR46892 on NTS1-$G\alpha_{i1}$ interactions.

2. Materials & Methods

2.1. Expression and purification of recombinant proteins

2.1.A) Expression: general points

All proteins were expressed in BL21(DE3) *E. coli*. Competent cells (Novagen) were transformed using a heat shock protocol (45s at 42°C, 2 min on ice). Shown in figure 10 are the details of each construct used.

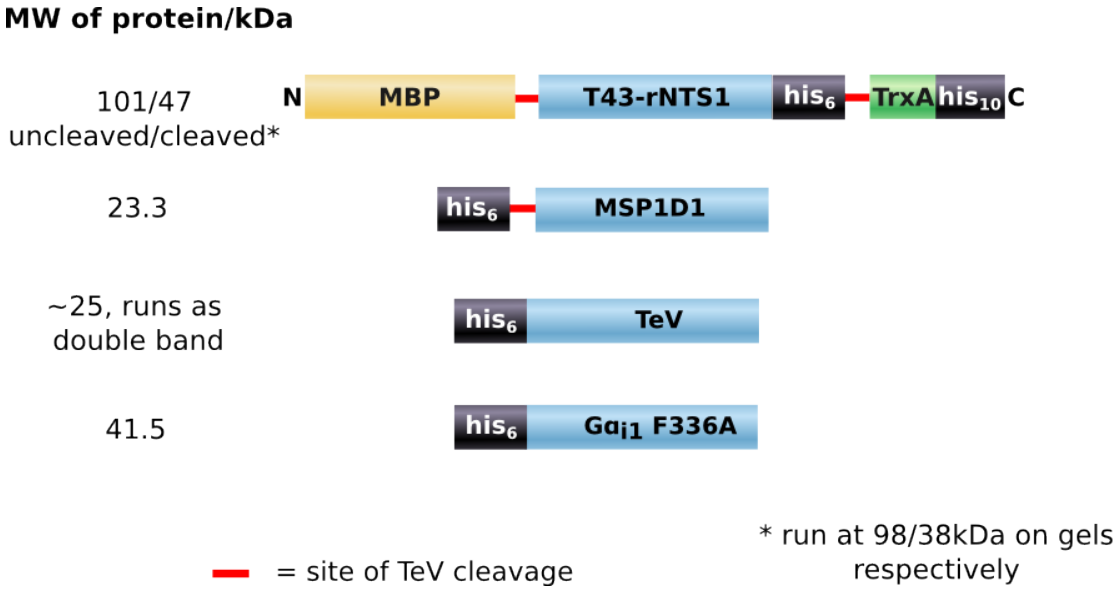

Figure 10: Constructs used in this dissertation. As noted, under the SDS-PAGE conditions used in this thesis, both uncleaved (NTS1B) and cleaved (NTS1) protein run at molecular weights smaller than their true molecular weights.

2.1.B) Purification: a schematic

Shown in figure 11 is the scheme used to purify the proteins used in this dissertation.

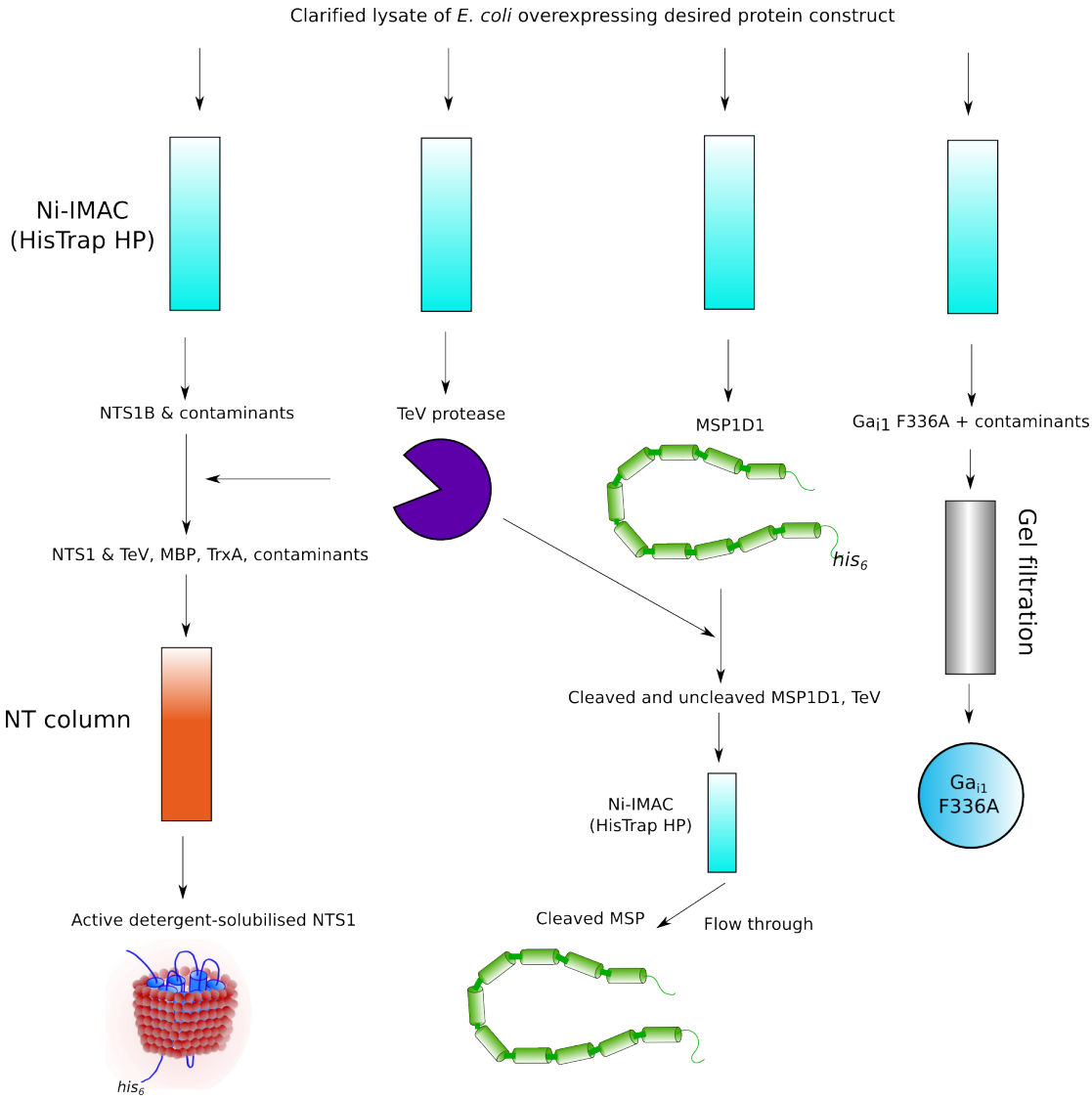

Figure 11: Purification schematic for NTS1, TeV protease, MSP1D1 and $G\alpha_{i1}$ F336A proteins. Image of detergent-solubilised NTS1 adapted from (Serebryany et al, 2012).

2.1.C) TeV PROTEASE EXPRESSION AND PURIFICATION

Single transformed colonies were picked and each added to 5ml Luria-Bertani broth and grown overnight at 200rpm and 37°C. The resulting cultures were mixed together before inoculation of 10L autoclaved 2x YT media (16g peptone, 10g yeast extract, 5g NaCl, per litre H_2O), followed by addition of kanamycin to 50µg/ml. Cells were grown at 37°C until reaching an optical density at 600nm (OD_{600}) of 0.25; the temperature was then reduced to 20°C. At OD_{600} of 0.6, cells were induced with 0.4mM Isopropyl β-D-1-thiogalactopyranoside and grown for 16-20 hours at 20°C. Cells were harvested by centrifugation (8,000g, 10 min, 4°C). The cell pellet was resuspended in 100ml equilibration buffer (table 4), 1mg DNAse was added and sample left to stir for 30 min at 4°C before being applied to a cell disruptor (constant systems TS series) at 25kPSI. Lysate was spun at 60,000g for 1hr and the supernatant filtered through 0.45µm syringe

filters. Before purification by immobilised-metal ion affinity-chromatography (IMAC), imidazole was added to a final concentration of 30mM. The sample was loaded onto a 5ml HisTrap HP column (GE Healthcare) equilibrated in equilibration buffer before washing with 25 column-volumes of wash buffer. Elution was achieved with elution buffer and fractions were collected and analysed for TeV content by SDS-PAGE. Selected fractions were pooled, diluted in storage buffer and concentrated to a suitable volume using Vivaspin centrifugal concentrators (10kDa molecular weight cut-off (MWCO)), before snap-freezing.

Buffer name	Components
Equilibration buffer	50mM Tris(hydroxymethyl)aminomethane (Tris), pH 7.4 300mM NaCl Protease inhibitors 1mg/ml lysozyme 5mM $MgCl_2$
Wash buffer	50mM Tris, pH 7.4 300mM NaCl 30mM Imidazole
Elution buffer	50mM Tris, pH 7.4 300mM NaCl 500mM Imidazole
Storage buffer	50mM Tris, pH 7.4 25% glycerol 150mM NaCl

Table 4: Buffers used in purification of TeV protease. Protease inhibitors = 2µg/ml pepstatin & leupeptin, 0.3µg/ml aprotinin.

2.1.D) MSP EXPRESSION AND PURIFICATION

The MSP1D1 construct (figure 10) was expressed and purified based on a protocol detailed in (Ritchie *et al*, 2009). In addition to the modifications described in (Adamson & Watts, 2014), the solubilised cell lysate was applied to a cell disruptor (constant systems TS series). Where necessary, the his_6-tag was cleaved by incubation with TeV in a 1:10 molar ratio of MSP:TeV plus 5mM dithiothreitol (DTT) overnight at 4°C. Cleaved MSP was purified by IMAC, whereby the cleavage mixture was loaded onto a 1ml HisTrap HP column equilibrated in TeV equilibration buffer and the flow through collected.

2.1.E) GAI1 EXPRESSION AND PURIFICATION

Purified wild type $G\alpha_{i1}$ protein was donated by Roslin Adamson. F336A $G\alpha_{i1}$ was expressed and purified as for the wild type protein described in (Greentree & Linder, 2004), except that BL21(DE3) *E. coli* were used for expression and a 5ml HisTrap HP was used for Ni-IMAC. Additionally, a gel filtration step was implemented; G protein was loaded onto a Superdex 200 16/100 XK column (GE healthcare) equilibrated in a buffer of 40mM phosphate, pH 7.4.

2.1.F) NTS1 EXPRESSION & PURIFICATION

For NTS1 expression, the construct used (figure 10), is based on that described in (Tucker & Grisshammer, 1996) with modifications.

Expression and IMAC stages of purification were carried out as described in (Attrill *et al*, 2009), but without phospholipids in buffers. In some cases, the cell lysate was applied to a cell disruptor at 25kPSI. IMAC elution fractions were analysed by SDS-PAGE and selected fractions were pooled, diluted to reduce [imidazole] below 100mM and incubated with TeV protease. This cleaves at the sites shown in figure 10, to leave NTS1 with a C-terminal his_6-tag. The resulting protein construct is more native-like since there are no additional polypeptides at the N and C termini. NTS1B was incubated with ~200nmol TeV protease per 10L preparation and 5mM DTT overnight at 4°C with rotation. Cleaved receptor was then subjected to an NT-affinity column, as detailed in (Attrill *et al*, 2009; Harding *et al*, 2009) except with 15% glycerol in buffers. Purified receptor was then concentrated with Vivaspin centrifugal concentrators (50kDa MWCO) or by loading onto a 1ml HisTrap-HP column. The column was equilibrated in NiA^0 buffer (50mM Tris, pH 7.4, 15% glycerol, 200 mM NaCl, 0.1% n-dodecyl-β-D-maltoside (DDM), 0.01% Cholesteryl hemisuccinate (CHS)), washed with ~50 column-volumes of this buffer and protein eluted into 0.5ml fractions using NiB buffer (as NiA^0 plus 500mM imidazole).

2.2. RECONSTITUTION OF NTS1 INTO NANODISCS

2.2.A) FROM PURIFIED, DETERGENT-SOLUBILISED RECEPTOR

The protocol used was adapted from that described in (Ritchie *et al*, 2009). Shown in table 5 are the optimal and actual values for various parameters that affect the efficiency of the nanodisc reconstitution. A film of brain polar lipid extract (BPL, Avanti) was prepared by evaporating the chloroform in which the lipids are solubilised; BPL solution is decanted into a round bottom flask, then placed on a rotary evaporator for 20 min and then left in a vacuum dessicator overnight. Lipid solubilisation buffer (100mM Na Cholate, 50mM NaCl, 1mM Ethylenediaminetetraacetate (EDTA)) was then added to create a lipid solution at a concentration of 50mM. Solubilisation is achieved by freeze-thaw cycles and sonication. Detergent-solubilised, purified NTS1 and solubilised lipid were mixed together at the desired ratio and incubated on ice for 15 min. Cleaved

MSP was then added to achieve the desired MSP:lipid:NTS1 ratio and incubated rotating at 4°C for 1hr. Fresh biobeads (BioRad) were washed in methanol, then water, then gel filtration buffer (50mM Tris, pH 7.4, 100mM NaCl, 5mM $MgCl_2$) and added to the mix at a ratio of 0.5-0.8g/ml suspension to remove detergent and drive nanodisc formation. This was incubated overnight with rotation at 4°C. Biobeads were then removed and fresh ones added and incubated for 1hr. These were removed to leave the nanodisc-containing sample.

Parameter	Optimal conditions	Actual conditions used for BPL-nanodiscs
[NTS1] (uM)	~1	1.7
[MSP] (uM)	~120-140	120
[Glycerol] (% v/v)	<4	2.1
[Cholate] (mM)	12-40	21
[Lipid] (mM)	4-18	8.3
MSP:lipid	Empirical	1:70
NTS1:MSP	Empirical	1:70

Table 5: parameters affecting efficiency of nanodisc reconstitution. Table based on (Ritchie *et al*, 2009)*. The last two parameters are empirical since they depend on the identity of the protein; different proteins displace different numbers of phospholipids in a loaded vs empty nanodisc* (Ritchie *et al*, 2009)*. In these cases, the ratios used were previously determined optima from the host laboratory. The large, 70-fold molar excess of MSP to NTS1 favours inclusion of NTS1 in nanodiscs as a monomer* (Ritchie *et al*, 2009; Glück *et al*, 2011).

Nanodiscs were then purified in a two-step process. Gel filtration separates nanodiscs from lipid aggregates. Before loading, sample was centrifuged for 10 min at 10,000g to remove unsolubilised material and filtered using Nanosep MF centrifugal filters 0.2 µm (PALL corporation). Sample was applied to a 10/30 Superdex-200 GL column (GE Healthcare) equilibrated in gel filtration buffer and fractions collected and analysed by SDS-PAGE. Selected fractions were pooled and loaded onto a 1ml HisTrap HP column equilibrated in gel filtration buffer, washed with 50 column-volumes gel filtration buffer and eluted in elution buffer (gel filtration buffer + 500mM Imidazole). This separates NTS1-nanodiscs from empty nanodiscs since the cleaved NTS1 has a his_6-tag.

2.2.B) FROM *E. COLI* MEMBRANES

A pellet of NTS1B-transformed BL21-cells was resuspended in resuspension-buffer (50mM Tris, pH 7.4, 1mM EDTA, protease inhibitors as for TeV purification) at a ratio of 2ml buffer/g cells. The sample was applied to a cell disruptor at 25kPSI, and then centrifuged at 10,000g for 10 min at 4°C. The supernatant was spun at 118,00g for 1hr at 4°C to pellet the membranes. For storage, the membranes were resuspended in resuspension buffer at a ratio of 2.5ml buffer/g pellet. To re-pellet membranes, they are again spun at 118,000g at 4°C for 30 min. The membranes were solubilised by addition of detergent-buffer (50mM Tris, pH 7.4, 200mM NaCl, 1% DDM) at a ratio of 2.5ml buffer/g pellet. This was incubated at 4°C with rotation for 1hr, before centrifugation at 12,000g for 30 min at 4°C to remove unsolubilised membranes.

Nanodiscs are then formed as for detergent-solubilised receptor, the only differences being that uncleaved MSP was used and both POPC and BPL nanodiscs were prepared. The sample was loaded onto a 1ml HisTrap HP column equilibrated in equilibration buffer (50mM Tris pH 7.4, 200mM NaCl, 0 or 30mM Imidazole), washed with 50 column-volumes of this buffer and eluted in elution buffer (as equilibration buffer but 500mM imidazole). Fractions were analysed for NTS1 content by SDS-PAGE and selected fractions were pooled and diluted in equilibration buffer to reduce [imidazole]<100mM. Gel filtration was then performed as described for detergent-solubilised receptor nanodiscs.

In some cases these nanodiscs were subjected to TeV cleavage, carried out as for detergent-solubilised receptor. For some samples an NT-affinity column was also used, using the same protocol as detergent-solubilised receptor but with buffers containing no detergents or glycerol.

2.3. BIOCHEMICAL TECHNIQUES

2.3.A) SDS-PAGE

SDS-PAGE was performed using NuPAGE products from Invitrogen; pre-made Bis-Tris 12% gels were run in MES running buffer. Generally 15µl of sample was added to 5µl of 4X LDS sample buffer plus 60mM DTT. Gels were run for 35-50 min at 180-200V and stained using PageBlue stain (Thermo scientific) or a silver stain plus kit (BioRad) for increased sensitivity. In some cases, ImageJ software was used to quantify intensities of bands on gels.

2.3.B) WESTERN BLOTS

Western blots were performed on SDS-PAGE gels blotted onto nitrocellulose membranes, using an anti-mouse WesternBreeze® Chromogenic Kit (Invitrogen) and an anti-MBP primary antibody (Sigma-Aldrich) at a 1:7000 dilution.

2.3.C) BCA ASSAY

For quantification of *E. coli* membrane protein concentration, a bicinchoninic acid (BCA) protein assay kit (Pierce) was used.

2.3.D) RADIOLIGAND-BINDING ASSAY

To determine NT-binding activity of NTS1 samples, a binding assay was performed using the radioligand ^{3}H-NT_{8-13} (New England Nuclear, specific activity 3.33TBq/mmol). ^{3}H-NT_{8-13} (5µl, 9nM) was added to 25µl of NTS1 at nanomolar concentrations. For measurement of non-specific binding, 2µl of 4µM unlabelled NT_{8-13} was also added, and in both cases the reaction mixture was topped up to 60µl with assay buffer (50mM Tris pH 7.4, 0.1% DDM, 0.01% CHS (w/v), 1mM EDTA, 0.1mg/mL bovine serum albumin). After a 1-hour incubation at 4^{o}C, P30 spin columns (Bio-Rad) were used to separate bound and unbound NT_{8-13} by gel filtration. Eluate was added to 5ml scintillation fluid (ScintiSafe 3, Fischer Scientific) in scintillation vials, mixed, and placed on a scintillation counter (Walla 1409 DSA Liquid Scintillation Counter, Perkin Elmer). Non-specific binding sample counts were subtracted to give counts arising from specific binding of ^{3}H-NT_{8-13} to NTS1.

2.4. BIOPHYSICAL TECHNIQUES

2.4.A) CIRCULAR DICHROISM

Circular dichroism (CD) spectra were obtained on a Jasco J-815 spectropolarimeter over a wavelength range of 190-260nm at 10nm/s. Ten traces were acquired per condition, and were corrected by subtraction of buffer traces and smoothened using a Savitzky-Golay filter (convolution width of 11). Proteins were diluted so that the maximal high tension voltage remained <600V.

2.4.B) FLUORESCENCE POLARISATION ASSAY

The GTP binding activity of G proteins was assayed using fluorescence-polarisation based saturation-binding experiments. BODIPY-Guanosine 5'-O-(3-thiotriphosphate) (BODIPY-GTP-γ-S) (Molecular Probes, Life Technologies) was used as a fluorescent, non-hydrolysable GTP analogue. G protein in 40mM phosphate, pH 7.4 was serially diluted to give 16 points and incubated with 25nM BODIPY-GTP-γ-S for 1hr in a 384-well microplate. For each G protein either duplicate or triplicates were made. In addition, duplicate incubations were made for each protein using both 25nM BODIPY-GTP-γ-S and 1mM unlabelled GTP-γ-S, to account for non-specific binding. A PheraSTAR microplate reader (BMG labtech) was used to measure end-point fluorescence polarisation at 520nm, at 10% gain with 50 milli-polarisation (mP) units. Data were analysed in GraphPad Prism 6.

2.4.C) SURFACE PLASMON RESONANCE

SPR experiments were carried out on a Biacore T200, following the protocol described in (Adamson & Watts, 2014). In brief, $G\alpha_{i1}$ (wild-type or F336A) was coupled to a Biacore CM5 chip using amine coupling. Flow cells 2, 3 & 4 were coupled, whilst flow cell 1 was activated and blocked as a reference cell. The experiments were performed using single-cycle kinetics programmes.

A serial dilution of loaded nanodiscs was used as the analyte (from 500nM to 31nM unless otherwise specified), and equivalent concentrations of empty BPL nanodiscs used as a buffer reference. Samples were flowed over all flow cells at a rate of 50µl/min with the path 2-1, 3-1, 4-1. Analysis temperature was 25°C in all cases, and the buffers used for preparation of sample and the running buffers were matched for each experimental condition (table 6).

Ligand-bound state of receptor	**Buffer composition**
Apo-receptor	50mM Tris, pH 7.4, 100mM NaCl, 5mM $MgCl_2$
NT_{8-13} bound	As for Apo-NTS1, plus 2µM NT_{8-13}
SR48692 bound	As for Apo-NTS1, plus 2µM SR48692

Table 6: SPR buffer compositions.

Data were analysed in Biacore BIAevaluation software. Firstly, experimental sensorgrams were double referenced - both the buffer references and reference flow cell data were subtracted. Corrected sensorgrams were then analysed by kinetic analysis, applying 1:1 langmuir and heterogeneous ligand-binding models to the fit.

3. Results

3.1. Expression & purification of MSP & TeV protease

The yield of MSP and TeV proteins obtained from single 10L preparations was sufficient for all the experiments described in this dissertation (figure 12).

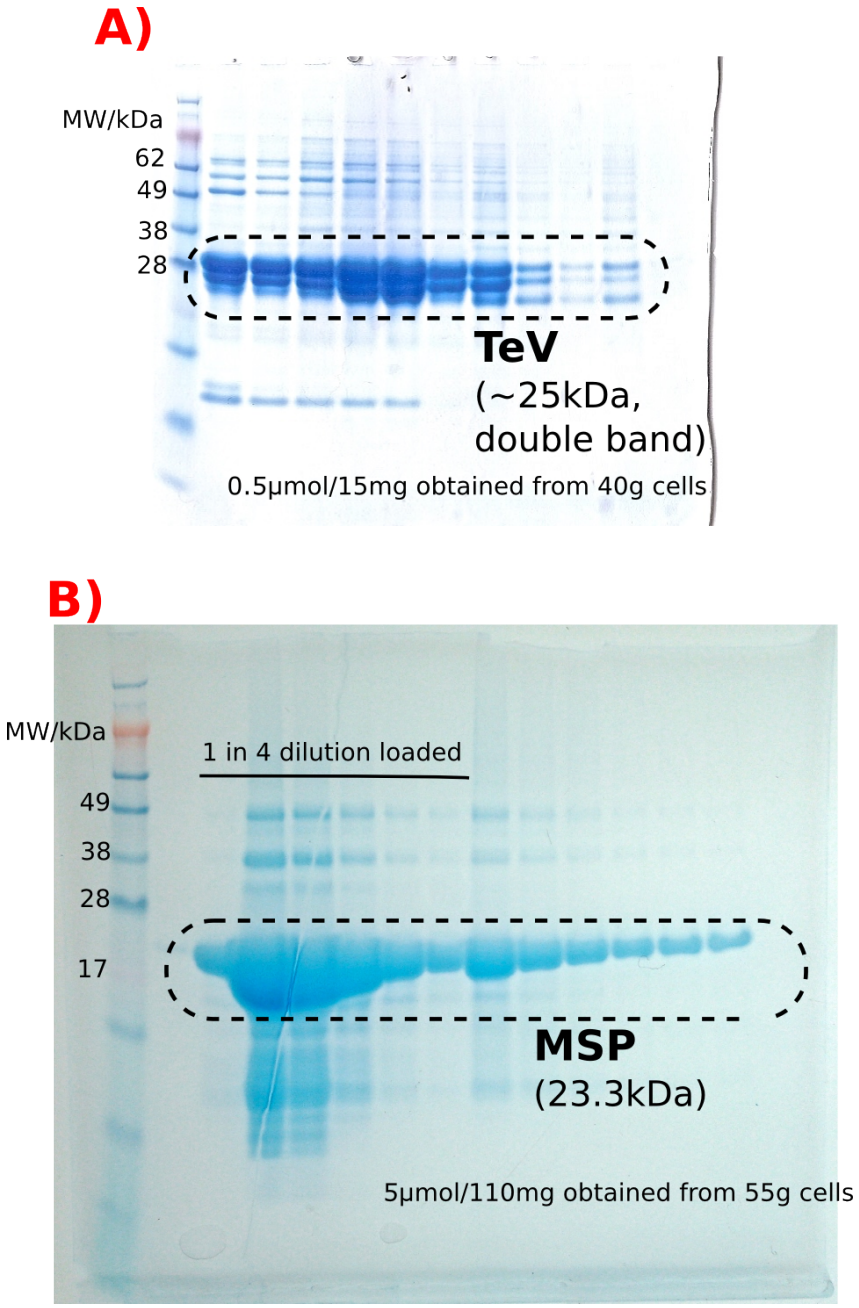

Figure 12: MSP & TeV purification. A summary of the A) TeV and B) MSP obtained by a single step IMAC purification protocol.

3.2. Expression, purification & reconstitution of NTS1

Shown in figure 13 is a schematic summary of the purification of detergent-solubilised NTS1, illustrated with typical results at each step.

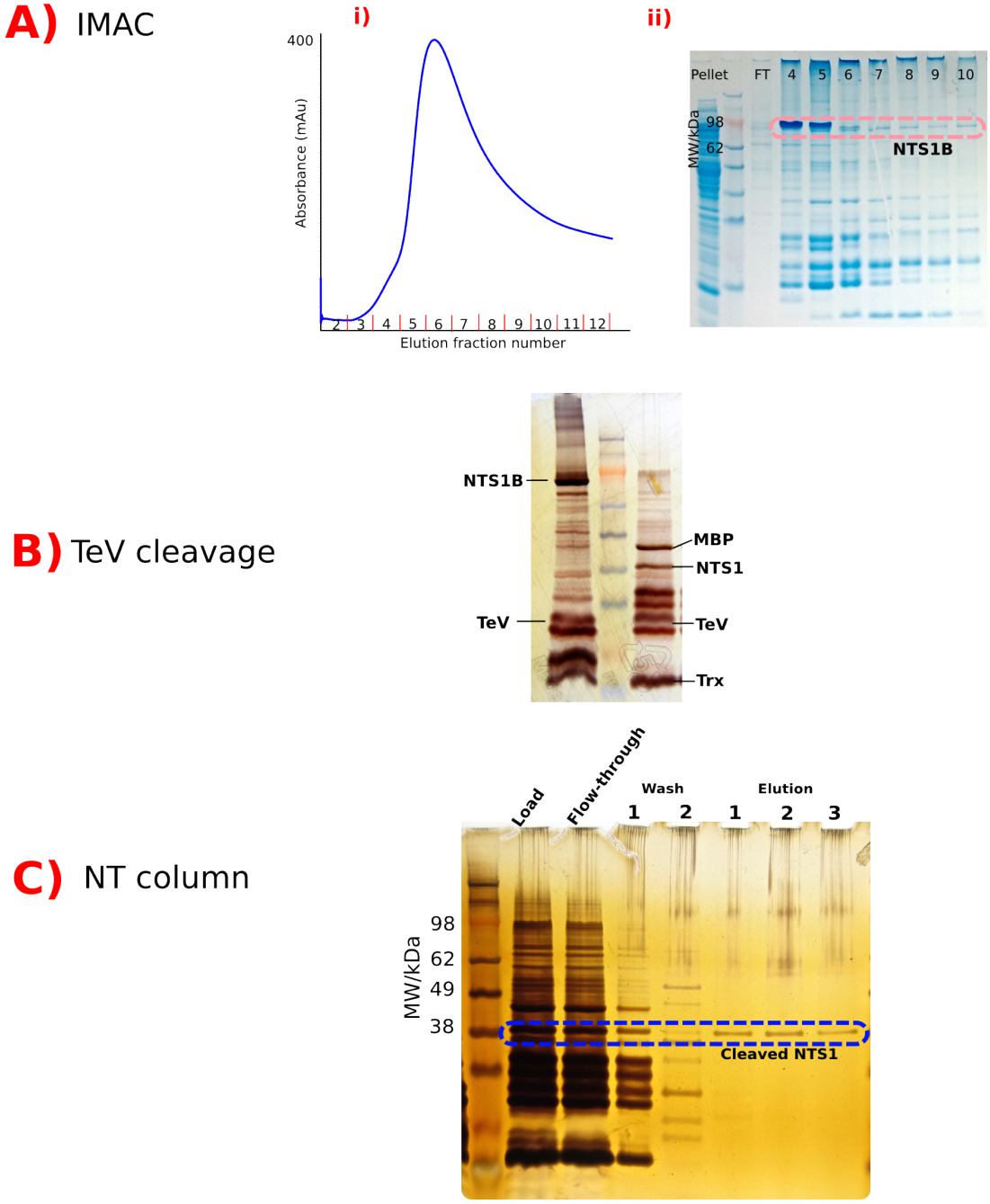

Figure 13: A summary of NTS1 purification A) IMAC of detergent solubilised lysate of NTS1-transformed E. coli, showing typical i) elution profile and ii) SDS-PAGE of elution fractions. B) TeV cleavage of NTS1. C) NT-affinity chromatography of cleaved NTS1.

Notably, there is far more NTS1 in the flow through of the NT-column than the elution (figure 13C). This is not an issue of column capacity (R dos Reis,

unpublished results, 2014), and this phenomenon has been noted and discussed previously by others (White & Grisshammer, 2010). Hence much of the NTS1 at this stage of the purification is inactive (with respect to NT-binding), and/or becomes inactivated by application to the NT-column. This is likely to be detergent induced, given the observed time-dependent loss of NT-binding activity in detergent described in (Oates *et al*, 2012); it is also suggested that close proximity of NTS1 to the resin on the NT column may contribute to inactivation (White & Grisshammer, 2010).

From each 10L preparation (40-80g cells), less than 1mg of pure NTS1 was obtained. As a result, two strategies were developed in an attempt to improve active receptor yield.

3.2.A) Use of cell disruptor

Firstly, the effect of a cell disruptor was tested, since the existing protocol relies on re-suspension of pelleted cells and addition of lysozyme (Attrill *et al*, 2009) for lysis; improved lysis from a harsher disruption method might yield more receptor. A preparation of NTS1-transformed BL21 cells was split into 2 aliquots after resuspension; one was immediately solubilised in detergent whilst the other was subjected to the cell disruptor first. Each was then independently purified using Ni-IMAC; gels were run and analysed for relative NTS1 content (figure 14). Radioligand-binding assays were then performed to analyse the activity of either sample, as summarised in table 7.

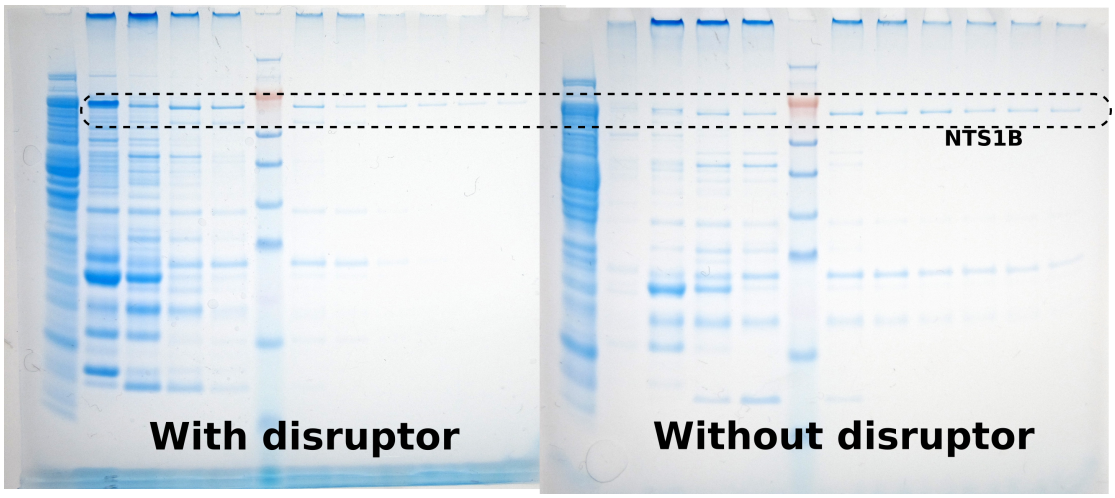

Figure 14: The effect of cell disruptor on NTS1 yield. Shown are SDS gels for NTS1B samples after IMAC, with or without the application of a cell disruptor. Both gels were subjected to equal running, staining and photographic recording conditions. These gels were analysed for NTS1 band intensity using ImageJ, to give a relative concentration for each sample, since the presence of contaminating proteins means absorbance at 280nm (A_{280}) is not a reliable measure of NTS1 concentration.

	With disruptor	Without disruptor
Relative [NTS1] from gels	1	1.22
Relative activity in assay samples	1	2.03
Relative activity of IMAC elution	1	2.48

Table 7: Relative activities of NTS1 samples with and without cell disruptor. Radioligand-binding assays were performed on IMAC samples diluted to the same concentration. The relative activity values are then compensated for the difference in NTS1 concentration in the IMAC elution (measured by ImageJ analysis of gels).

3.2.B) NANODISCS FROM *E. COLI* MEMBRANES

Since the loss of NTS1 is likely to be at least in part detergent-induced, an alternative approach to nanodisc formation was trialled. Membranes of NTS1-transformed *E. coli* were isolated and solubilised, and nanodiscs formed from them, rather than from detergent-solubilised receptor. This way, NTS1 can be purified in nanodiscs rather than detergent, minimising detergent exposure and placing NTS1 in a lipid environment early in the purification procedure.

A limited precedent for such an approach exists. Direct formation of cytochrome P450 nanodiscs from *Spodoptera frugiperda* membranes and subsequent purification is described in (Civjan *et al*, 2003), whilst in (Marty *et al*, 2013) nanodiscs were used for solubilisation of the *E. coli* membrane proteome from a membrane preparation. Most notably, a class B GPCR has also been reconstituted into nanodiscs from solubilised Human embryonic kidney-293 cell membranes, with the nanodiscs being subsequently purified (Mitra *et al*, 2013).

As described in (Ritchie *et al*, 2009), one must consider the contribution of endogenous lipids when forming nanodiscs - an excess of exogenous lipid should be added to minimise the contribution of endogenous lipids. The MSP:lipid ratio is an important consideration, since too little lipid gives a poor nanodisc yield and too much gives large lipid aggregate species (Marty *et al*, 2013). A molar ratio of approximately 1:90 MSP:lipid was chosen after (Mitra *et al*, 2013; Marty *et al*, 2013) and an additional ratio of 1:150 MSP:lipid was also tested. POPC or BPL lipids were chosen as the exogenous lipid; NTS1 shows favourable activity characteristics in the latter (Oates *et al*, 2012), whilst the former gave efficient nanodisc formation from *E. coli* membranes in (Marty *et al*, 2013). The second ratio to consider is MSP:membrane protein; since there is no way of selectively reconstituting NTS1 into nanodiscs over other membrane proteins present, one must estimate the total membrane protein content of the membranes. Using a BCA assay, this was determined at 6.5±0.5 mg/ml. A ratio

of 1nmol MSP: 10ug membrane protein was decided, after (Marty *et al*, 2013; Mitra *et al*, 2013).

Purification of these nanodiscs is summarised in figure 15.

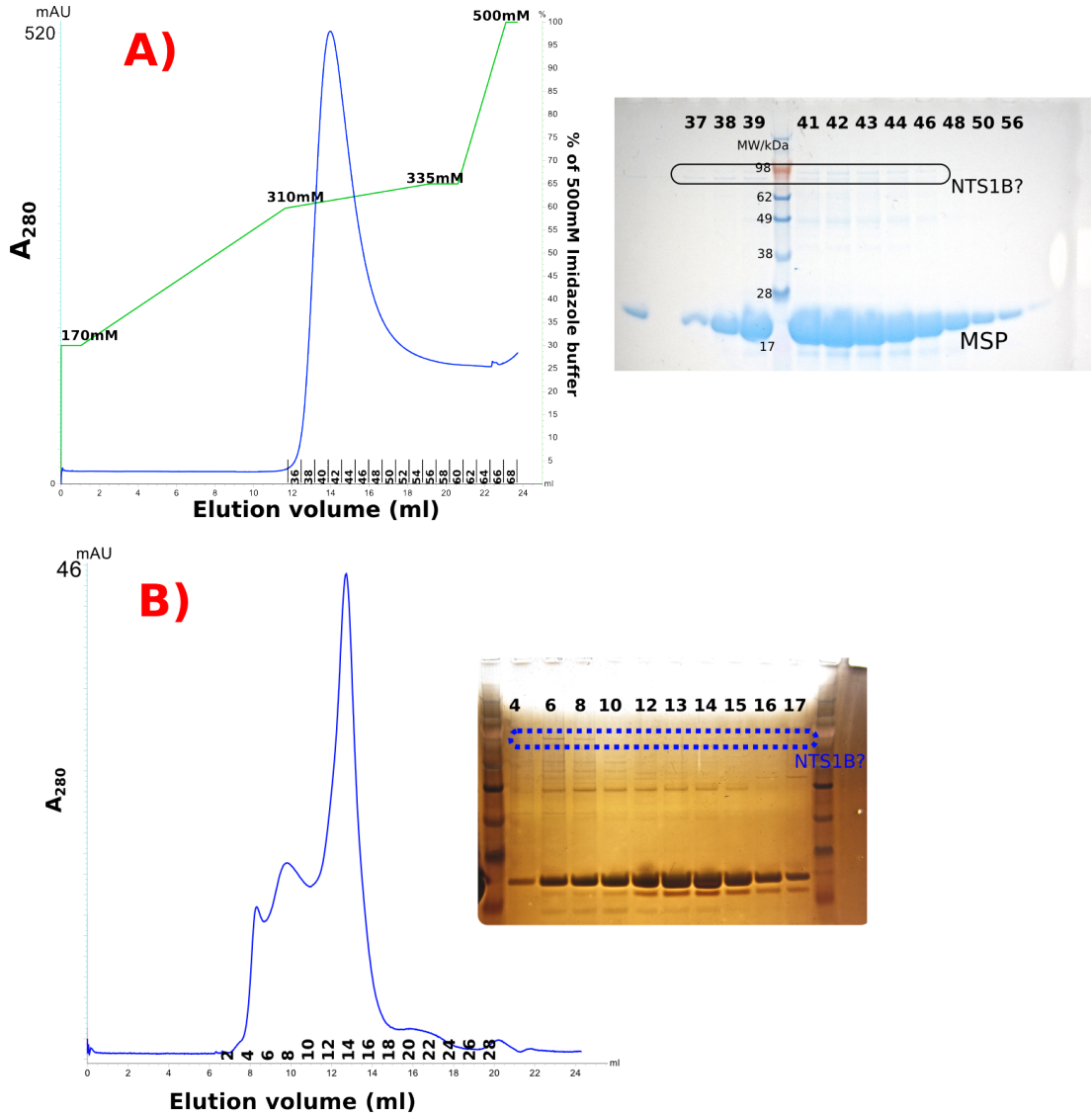

Figure 15: Purification schematic for nanodiscs formed from E. coli membranes, with POPC nanodiscs at 90:1 POPC:MSP as an example. A) IMAC using linear gradients of imidazole was used in an attempt to separate NTS1-nanodiscs from other nanodiscs; the former has his-tags from both NTS1 and MSP, whilst nanodiscs that are empty or contain other proteins possess only the MSP his-tag. B) Gel filtration; employed to remove free MSP and further separate loaded and empty nanodiscs. In some cases, a NT column was applied after this step (not shown) for further purification and to test the NT-binding of the sample.

A band consistent with NTS1B is present at low intensities before and after gel filtration (figure 15A,B). Several approaches were taken to ascertain if NTS1B was present in the purified product. Shown in figure 16 is a western blot

performed on selected samples after gel filtration using an anti-MBP primary antibody (which detects the uncleaved receptor). As can be seen, no band was detected for any of the nanodisc preparations despite a positive control being detected. Moreover, for all samples, no NT-binding activity was detectable; those samples applied to an NT-column appeared in the flow-through, and no specific counts were detected with a radioligand-binding assay.

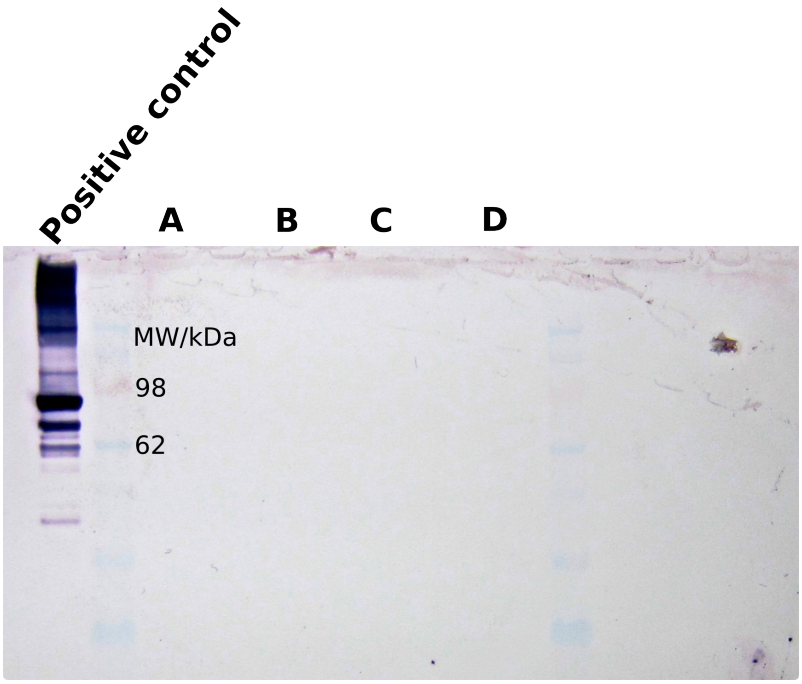

Figure 16: Anti-MBP western blot of purified nanodisc samples. The positive control used was the IMAC elution from a preparation of detergent solubilised-NTS1. A, B= different preparations of nanodiscs using a 150:1 POPC:MSP ratio, C= 90:1 POPC:MSP nanodiscs, D=150:1 BPL:MSP nanodiscs.

3.2.C) Reconstitution of detergent-solubilised NTS1 into BPL nanodiscs

The production of NTS1-nanodiscs was not efficient, with a large gel filtration peak at low elution volumes (figure 17), consistent with a high concentration of lipid aggregates (Marty *et al*, 2013). The later peak is at an elution volume consistent with BPL-nanodiscs (P Dijkman, unpublished results, 2014).

Indeed, when solubilising the BPL lipids, it was noted that the solution remained cloudy and a large pellet formed during centrifugation of the sample, suggesting that the solubilisation of lipids was inefficient.

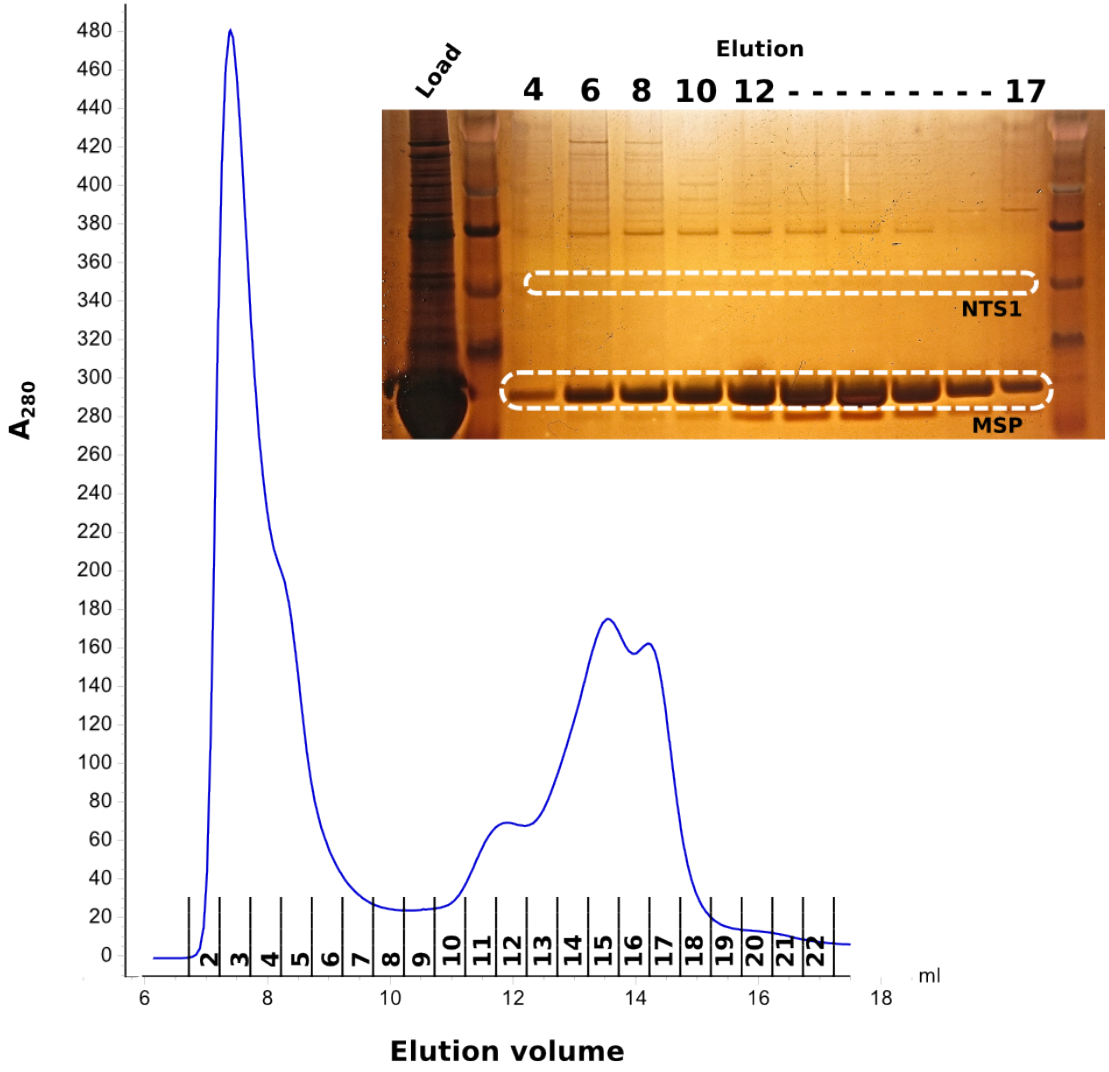

Figure 17: Gel filtration of nanodisc reconstitution mixture. Fractions from the late peak were pooled and purified further by IMAC. Shown alongside is a silver-stained SDS-PAGE gel of the gel-filtration fractions.

The concentration of nanodiscs after IMAC measured by A_{280} was estimated at 2µM. However, the NTS1 band is not clearly visible with silver-stained SDS-PAGE before (figure 17) or after IMAC; previous reconstitutions suggest that this band should be visible (Adamson & Watts, 2014). Nonetheless, specific NT-binding is detected by radioligand-binding assay and gives an active NTS1 concentration of 1.60±0.09nM. This value almost certainly underestimates NTS1 content, since the radioligand-binding assay used is not optimized for nanodiscs, and typically fails to show any specific NT-binding for POPC-POPG NTS1 nanodiscs (Personal communication, Roslin Adamson 2015). The poor visibility of NTS1 on gels could be explained by the presence of empty nanodiscs in addition to NTS1-nanodiscs. There is the possibility of poor separation of cleaved-MSP from his_6-MSP by IMAC, which would give rise to tagged empty-nanodiscs that co-elute with loaded nanodiscs during IMAC. Indeed, in figure 17,

one can see a double band at MSP for certain fractions, suggesting the presence of two MSP species. Moreover, empty nanodiscs have been observed to bind to Ni-columns even when his_6-MSP is completely cleaved (R Adamson, unpublished data, 2014). Hence the NTS1-nanodisc concentration has some uncertainty, but observation of NT-binding in BPL-nanodiscs is an improvement on POPC-POPG nanodiscs.

3.3. EXPRESSION & PURIFICATION OF $G\alpha_{i1}$ F336A MUTANT

Approximately 10nmol protein was obtained from a 10L expression culture (100g cells). Shown in figure 18 are results from the two purification steps used.

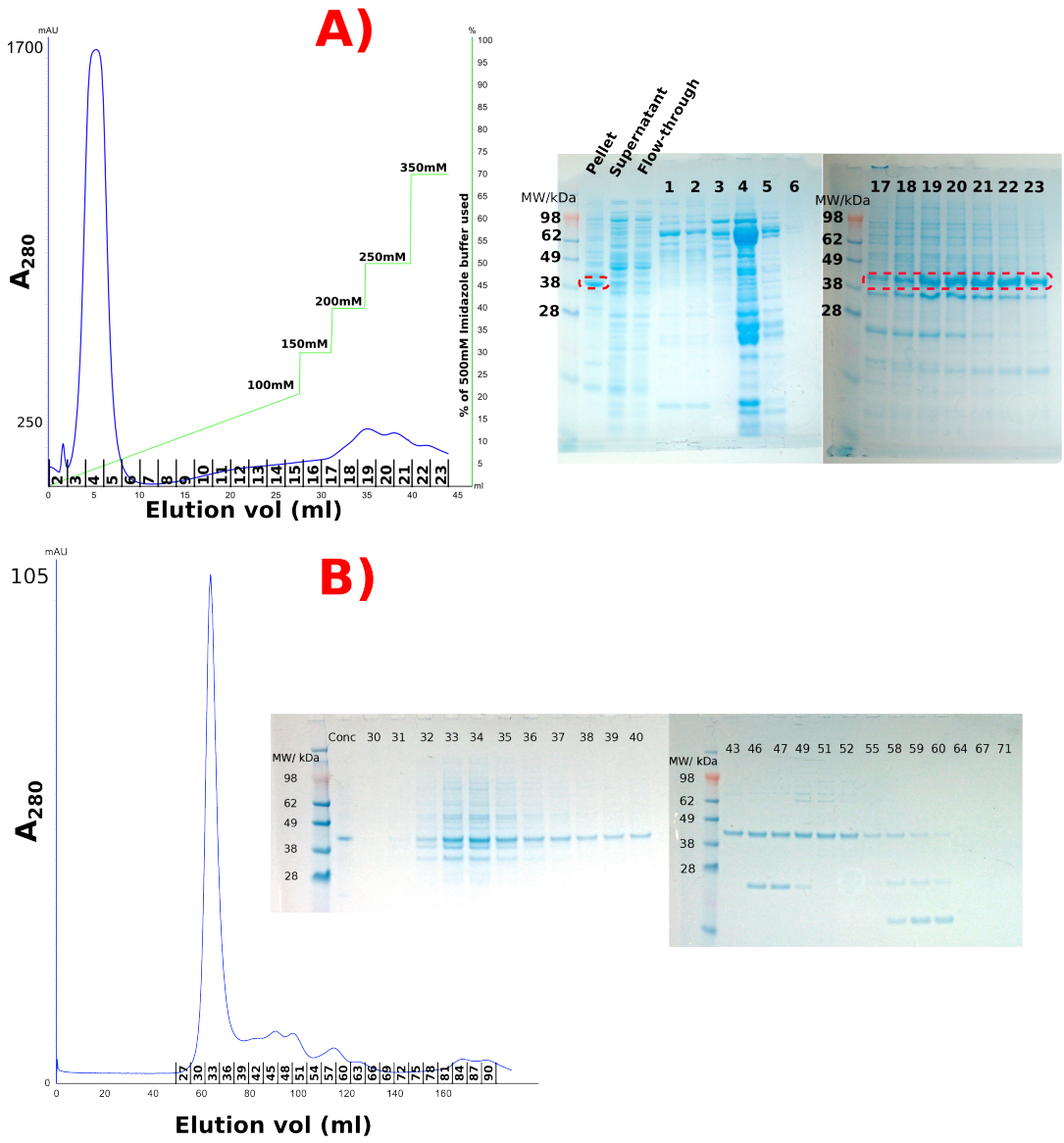

Figure 18: Purification of $G\alpha_{i1}$ F336A. Shown are results from A) IMAC and B) Gel filtration steps.

Purity after IMAC was poor, so gel filtration was also used. Contaminants were largely removed in this manner, but the large volume range over which the G protein elutes is concerning; wild type G protein elution occurs over a more defined volume range (R Adamson, unpublished data, 2014). Consistent explanations are that either the column is faulty, or the G protein is present in different states (e.g. folded and unfolded), which interact differently with the gel filtration matrix.

3.3.A) Assaying G protein folding and GTP binding activity

CD spectra were obtained for both F336A and wild-type $G\alpha_{i1}$, to test if the purified F336A protein was folded (figure 19).

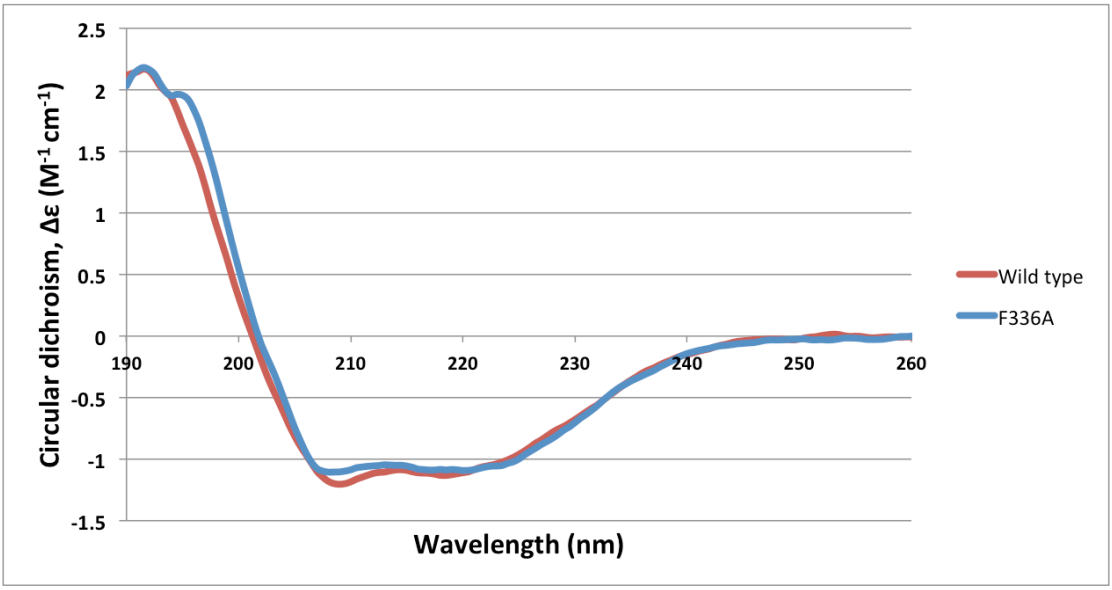

Figure 19: CD of G proteins. Overlaid CD spectra of wild type and F336A Gαi1 protein.

The spectra are near-identical, showing that both proteins have similar secondary-structure content and so are similarly folded. As an additional assay for folding/activity, affinity of F336A and wild-type $G\alpha_{i1}$ for BODIPY-GTP-γ-S was measured using a fluorescence polarisation assay. The result for wild type protein is shown in figure 20.

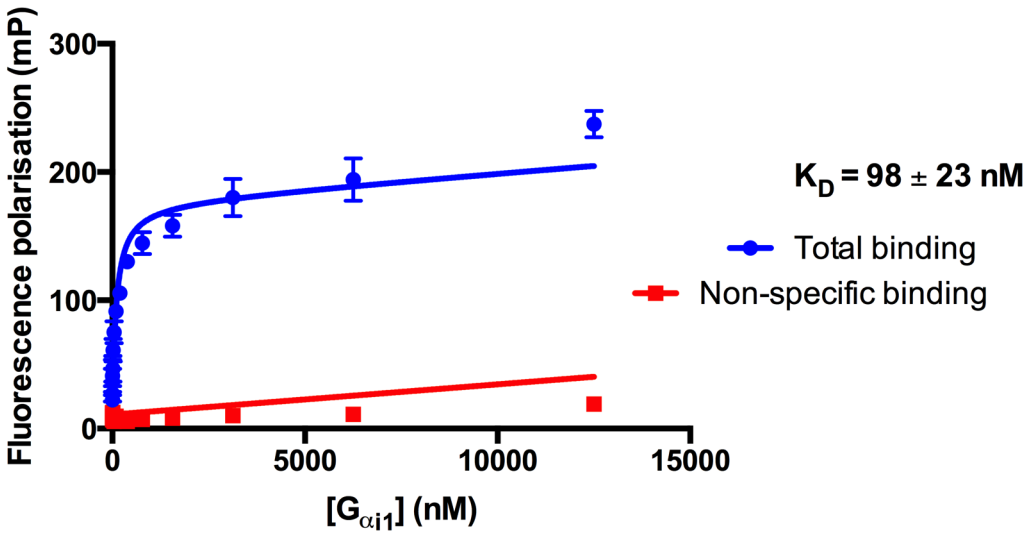

Figure 20: $G\alpha_{i1}$ affinity for BODIPY-GTP-γ-S. Shown is the K_D for the interaction of BODIPY-GTP-γ-S with $G\alpha_{i1}$ wild-type protein, determined by end-point fluorescence polarisation. Data were fit to an equation describing binding to a single site and total and non-specific binding were analysed globally using GraphPad Prism 6.

This result is consistent with a published value for this interaction of 150±50nM (McEwen *et al*, 2001). For the mutant, there was no significant difference between the values obtained for specific and non-specific binding. Nonetheless, the mutant shows a CD spectrum very similar to that of wild-type protein, which binds GTP as expected. This is consistent with both proteins sharing a similar global fold, but with local perturbations caused by the F336A mutation rendering it unable to bind GTP to an extent measurable by the assay used.

3.4. NTS1- $G_{A_{i1}}$ INTERACTIONS

The response recorded for immobilisation of G protein for different experiments is given in table 8.

Ligand-bound state of receptor	**G protein**	**Immobilisation response (RU)**
Apo	Wild-type	4330
	F336A	3250
NT_{8-13} bound	Wild-type	3290
	F336A	2920
	F336A replicate	2120
SR48692 bound	Wild-type	4220
	F336A	2220

Table 8: Response recorded from immobilisation of G protein to CM5 chip by amine coupling.

3.4.A) IN THE PRESENCE OF SR48692

Figure 21 shows the sensorgram obtained for the interaction between SR48692-bound NTS1 and wild-type $G\alpha_{i1}$, whilst table 9 presents the parameters derived from the heterogeneous ligand model fit to this data. This model fits the data well, with some deviations (figure 21B) but with residuals largely within the acceptable $\pm$ 2RU suggested in (Drescher *et al*, 2009) (figure 21C). The 1:1 model is less appropriate, deviating more significantly from the observed response and showing larger residuals (figure 21C). This suggests that the observed response results from at least two independent interactions – i.e. that there is heterogeneity in the analyte and/or ligand. Heterogeneity in the ligand population could arise from amine coupling of the G protein (section 1.5.B), whilst any empty nanodiscs present in the NTS1-nanodisc sample (section 3.2.C) would give rise to heterogeneity in the analyte.

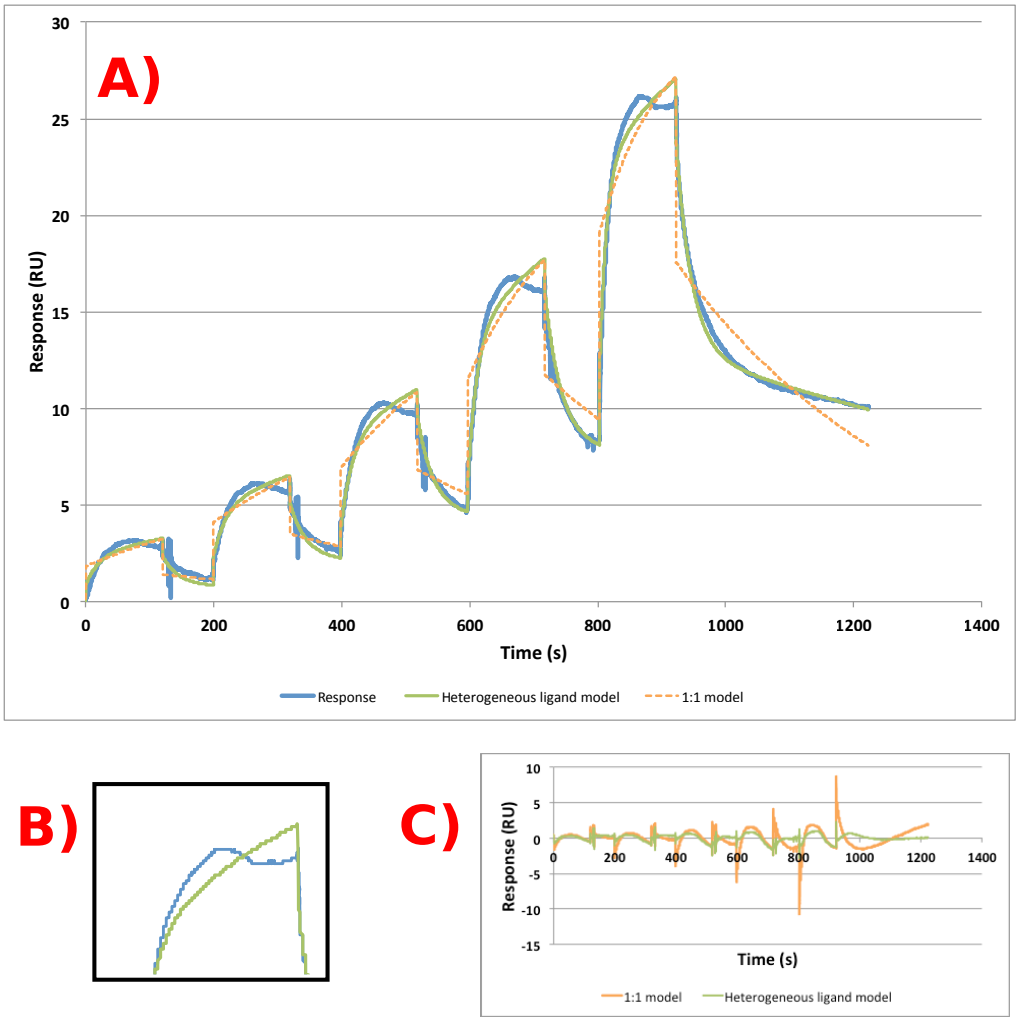

Figure 21: A) SPR results for the NTS1-Gα_{i1} (wild type) interaction, in the presence of SR48692. A) Shown is the experimental response overlaid by the fitted response generated by 2 different binding models using BiaEVALUATION software (Biacore). B) Magnified view of the fit provided by the heterogeneous ligand model around the maximal response at highest analyte concentration. C) Plots of residuals for different fitted responses.

The sensorgram for the NTS1-Gα_{i1} F336A interaction in the presence of SR48692 (figure 22) was poorly fit by a 1:1 model (not shown) and better fit with the heterogeneous ligand model. The fit in the dissociation regions of the curves, however, shows more deviation from the observed response than figure 21. This is highlighted by the fact that, as shown in table 10, the reported error on the k_d1 parameter is 478%.

Parameter	Value	SE	% error
k_{a1} ($M^{-1}s^{-1}$)	1.32×10^{4}	1.29×10^{2}	0.98
k_{d1} (s^{-1})	8.87×10^{-4}	1.42×10^{-5}	1.6
K_D1 (M)	6.74×10^{-8}		
R_{max} 1 (RU)	18.7	0.11	0.58
k_a2 ($M^{-1}s^{-1}$)	1.19×10^{5}	1.81×10^{3}	1.5
k_d2 (s^{-1})	4.17×10^{-2}	4.11×10^{-4}	0.99
K_D2 (M)	3.51×10^{-7}		
R_{max} 2	18.4	0.18	0.95
Chi^2 (RU^2)	0.238		

Table 9: Parameters obtained for the NTS1-Gα_{i1} wild-type interaction in the presence of SR48692. Values are derived from kinetic analysis of the fitted response generated by a heterogeneous ligand model, using BiaEVALUATION software (Biacore). SE=standard error reported by software.

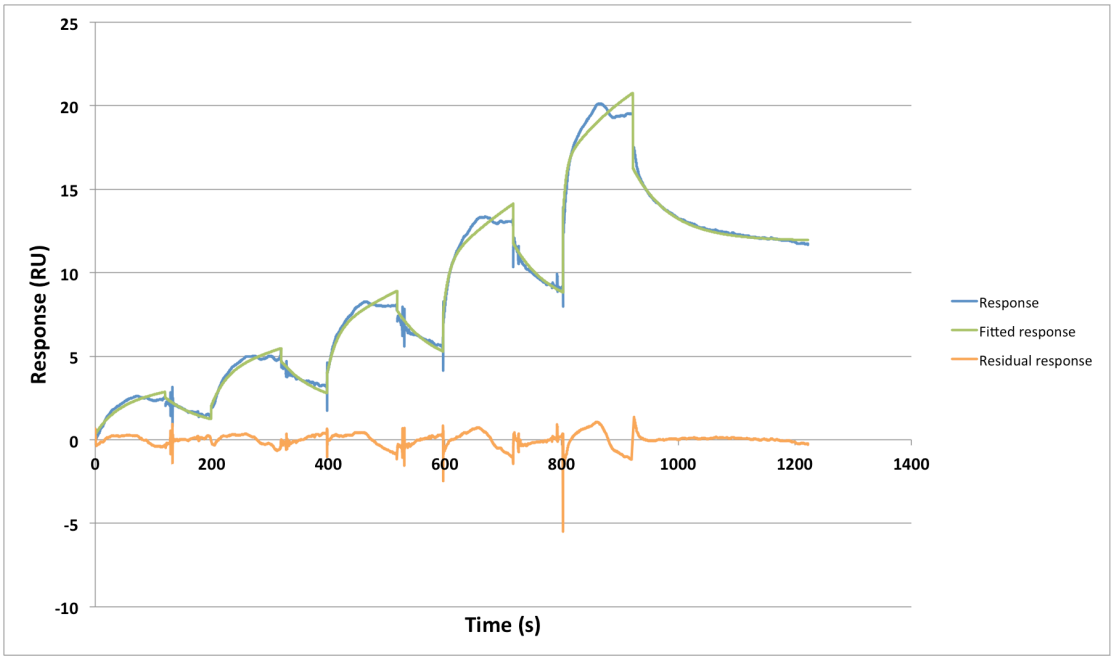

Figure 22: Sensorgram for the interaction between NTS1 and Gα_{i1} F336A in the presence of SR48692. Shown is the fitted response obtained by a heterogeneous ligand model and the residual response using this model.

Parameter	Value	SE	% error
k_{a1} ($M^{-1}s^{-1}$)	1.19×10^{4}	95	0.80
k_{d1} (s^{-1})	6.91×10^{-7}	3.30×10^{-6}	478
K_D1 (M)	5.82×10^{-11}		
R_{max} 1 (RU)	15.9	0.05	0.34
k_a2 ($M^{-1}s^{-1}$)	3.41×10^{5}	5.70×10^{3}	1.67
k_d2 (s^{-1})	1.55×10^{-2}	1.70×10^{-4}	1.10
K_D2 (M)	4.53×10^{-8}		
R_{max} 2	4.73	0.18	0.95
Chi^2 (RU^2)	0.132		

Table 10: Parameters obtained for the NTS1-$G\alpha_{i1}$ F336A interaction in the presence of SR48692. Values are derived from kinetic analysis of heterogeneous ligand fit. SE=standard error reported by software.

3.4.B) In the presence and absence of NT_{8-13}

The sensorgram for NT_{8-13}-NTS1 interacting with wild type $G\alpha_{i1}$ (figure 23) is given as a typical example of apo-NTS1 and NT_{8-13}-NTS1 interactions with both wild-type and F336A G protein observed.

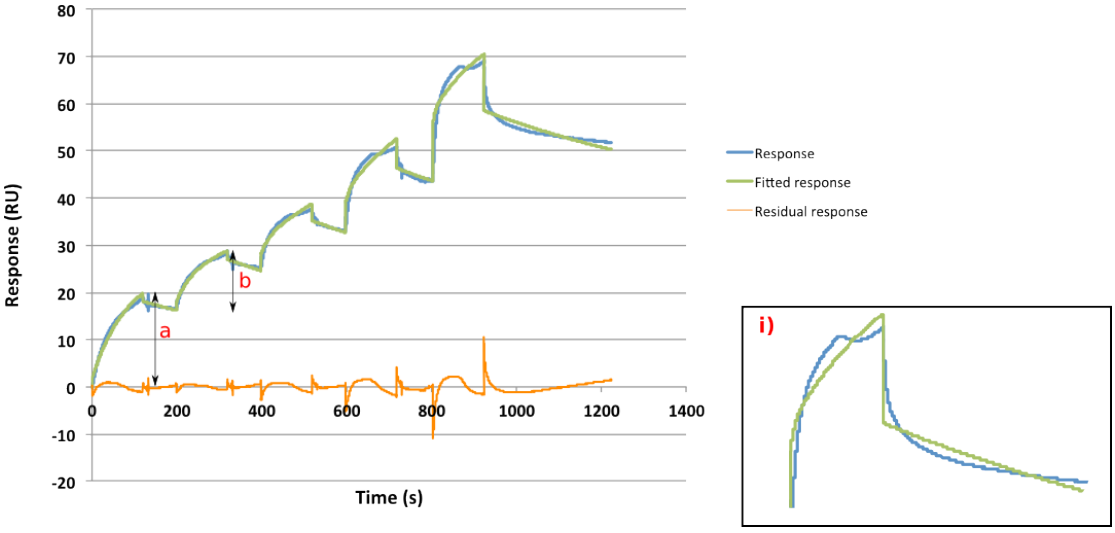

Figure 23: Sensorgram for the NTS1- $G\alpha_{i1}$ WT interaction in the presence of NT_{8-13}. Shown is the experimental response, the fitted response using a heterogeneous ligand binding model, and the residual response. Shown in the insert, i), is a close up of the response at the highest analyte concentration. Annotations a) and b) show the responses generated for the first and second analyte injections, respectively.

As for the SR48692 data, the NT_{8-13}- and Apo-receptor sensorgrams gave a poor fit with a 1:1 binding model (not shown). The heterogeneous ligand model gives a better fit, but there are significant deviations from the observed response (figure 23; residuals and inset). Most notably, the pattern of response in figure 23 with successive analyte injections/increasing analyte concentrations is

unusual. The response difference shown in figure 23a, for the first analyte injection (i.e. lowest analyte concentration) is larger than the response difference shown in figure 23b for the next analyte injection. This contrasts with the response seen with successive injections in figures 9, 21 & 22. Interestingly, after the second injection, the size of the successive responses increases again. This is consistent with a high-affinity binding site approaching or reaching saturation during the first injection, with successive injections leading to binding at a second, lower-affinity site. In such a hypothesis, the high-affinity binding site could represent the NTS1-$G\alpha_{i1}$ interaction of interest, with the lower-affinity interaction potentially arising from non-specific interactions between NTS1-$G\alpha_{i1}$ or between $G\alpha_{i1}$ and empty nanodiscs.

To test this hypothesis, an experiment was run with lower analyte concentrations (figure 24).

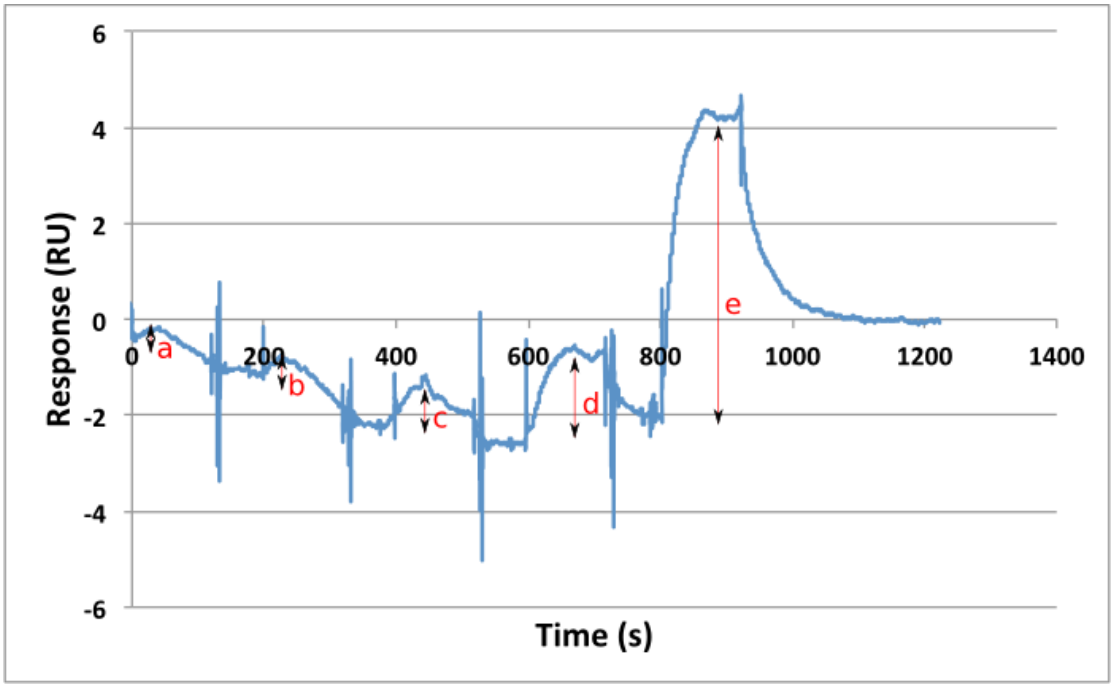

Figure 24: SPR results for NTS1-$G\alpha_{i1}$ wild type interaction in the presence of NT_{8-13} at lower analyte concentration. Here, a 5-point dilution series of analyte with a concentration range of 200nM to 13nM was used. Shown by (a) through (e) are the responses due to each successive analyte injection.

Encouragingly, the pattern of response with increasing concentration is more similar to figure 21/22 than figure 23 (in figure 24, a<b<c<d<e). Hence this supports the idea of (near-)saturation of NTS1-$G\alpha_{i1}$ binding at the lowest analyte concentration used in earlier experiments. Note that baseline drift means that this sensorgram cannot be fit to a binding model.

3.4.C) A COMPARATIVE APPROACH

Since the response at lowest analyte concentration is proposed to reflect an NTS1-Gα_{i1} interaction for each condition, comparative information can be deduced by using the maximal response at this analyte concentration for each condition (figure 25).

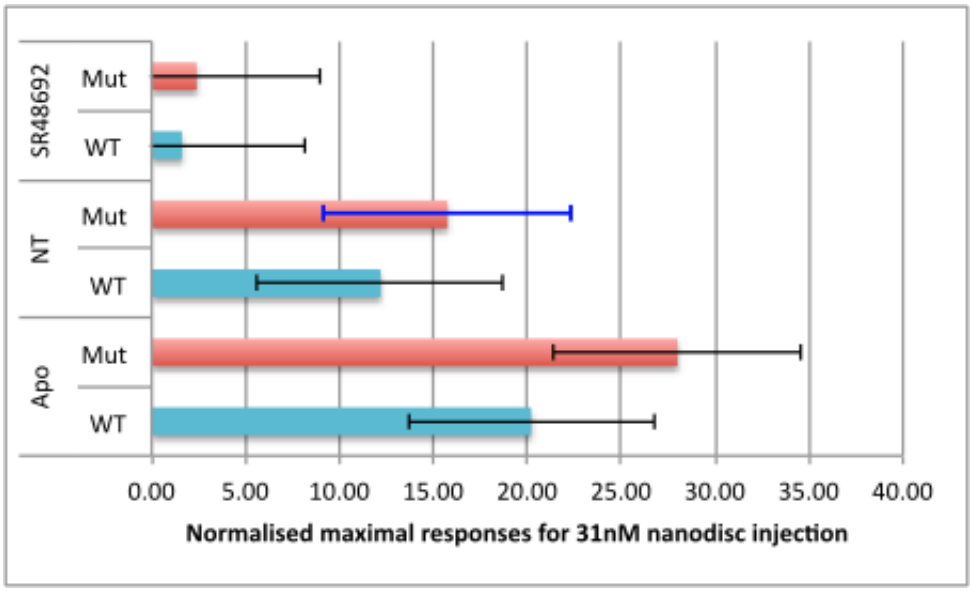

Figure 25: Comparison of normalised responses at lowest analyte concentration. WT and Mut refer to wild type and F336A Gα_{i1} protein immobilised on the chip surface, respectively. For each condition, the maximal response obtained in the 1st cycle (injection of nanodiscs at 31nM) is taken. These values are then adjusted for the relative amount of G protein immobilised for each condition (see table 8), to allow for direct comparison of responses. Due to time constraints, a replicate experiment was only performed for the "NT-Mut" condition; the calculated 95% confidence limits are shown as the blue error bar. Since this is the only error available, these limits have also been applied to the other conditions, shown as black error bars.

4. DISCUSSION

4.1. PRODUCTION OF NTS1-NANODISCS

NTS1 was successfully reconstituted into BPL-nanodiscs, with measurable NT-binding activity, representing an improvement on POPC-POPG nanodiscs used previously (Adamson & Watts, 2014). However, the yield of both active receptor and BPL nanodiscs was lower than anticipated.

The BPL-nanodisc reconstitution efficiency may be limited by solubilisation of the lipids and so could be improved in the immediate future by trialling different solubilisation conditions – for example, different concentrations of cholate, or by using a different solubilising detergent entirely.

In terms of active NTS1 yield, this was not improved by application of a cell disruptor to resuspended cells. Attempts to reconstitute NTS1 into nanodiscs from solubilised *E. coli* membranes were unsuccessful – however, since such an approach has successfully been applied to a GPCR before (Mitra *et al*, 2013) this approach is worth pursuing. All preparations of such nanodiscs were derived from the same batch of membranes; the cells from which these membranes were derived may have poorly expressed NTS1B. Repetition of the experiments described with a new batch of cells and anti-MBP western blots employed at each stage of the process (on detergent-solubilised membranes, after nanodisc reconstitution and after each purification step) would allow assessment of whether NTS1B is present at any of the stages.

In addition, a new method for purification of thermostabilised NTS1 mutants has been described recently (Egloff *et al*, 2014a), which allows for purification of NTS1 in a single step, requiring a single day. Implementation of this protocol for NTS1B might yield improved active NTS1 since it should reduce the time NTS1 spends in detergent and allow reconstitution into nanodiscs sooner after detergent-solubilisation of the receptor.

4.2 NTS1- G_{i1} INTERACTIONS

For the first time, NTS1 was assayed for interaction with $G\alpha_{i1}$ proteins by SPR in BPL-nanodiscs, under three different ligand-bound states of the receptor. This was conducted with both donated wild type $G\alpha_{i1}$, and F336A $G\alpha_{i1}$ that was successfully expressed and purified. Both G proteins appeared to be folded prior to immobilisation, although no GTP binding activity could be detected in the mutant.

4.2.A) SR48692 IS AN INVERSE AGONIST

Novel results were obtained for the NTS1- $G\alpha_{i1}$ wild-type interaction in the presence of SR48692. The parameters derived from the heterogeneous ligand model (table 9) describe two independent binding events, with similar

occupancy ($R_{max}1 \approx R_{max}2$) and K_D values of 67nM (interaction 1) and 350nM (interaction 2). An average K_D, weighted using R_{max} values, of 210nM, is comparable with the K_D of 300nM previously obtained for another GPCR-G protein interaction in the presence of antagonist (table 1, (Alves *et al*, 2003)). Potential heterogeneity in the analyte (section 3.2.C) means the concentration of the analyte of interest, the NTS1-nanodiscs, is uncertain. Consequently the k_{on} parameters (which are dependent on [analyte]) derived from these fits and the K_D values, which are derived in turn from k_{on} and k_{off}, are potentially higher than the true values for the NTS1-$G\alpha_{i1}$ interaction; 210nM should be considered an upper limit to the K_D. A similar analysis for the corresponding interaction with F336A $G\alpha_{i1}$ cannot be performed, since the error on k_d1 is prohibitively high (table 10) and the interaction to which it corresponds (1) is dominant ($R_{max}1>R_{max}2$).

Comparison of normalised responses (figure 25) suggests that SR48692 is acting as an inverse agonist. A true antagonist has no effect on the number of receptor states capable of G protein coupling and simply blocks binding of other ligands (figure 3) - so should not affect the affinity of a GPCR-G protein interaction. Assuming that the error calculated for the single replicate experiment (fig 25) is typical, and that the same binding site is involved for all conditions, then figure 25 shows that the SR48692-bound receptor binds $G\alpha_{i1}$ with lower affinity than the Apo-receptor. This result is consistent with previous experiments which find SR48692 to act as an inverse agonist on an NTS1 mutant with high constitutive activity (Barroso et al., 2002). Moreover, this result strongly suggests that the SPR system being used is able to detect specific NTS1- $G\alpha_{i1}$ interactions, since the response changes in the presence of a ligand specific for one component of the system.

4.2.B) AN F336A MUTATION IN $G\alpha_{i1}$ DOES NOT AFFECT GPCR BINDING

Making the same assumptions described in the previous section, the results for wild type and F336A $G\alpha_{i1}$ are not significantly different for each ligand-bound state of the receptor (figure 25). If these assumptions are valid, then mutating F336 to alanine does not significantly affect the affinity of the NTS1-$G\alpha_{i1}$ interaction for various ligand-bound states of the receptor. One explanation is that NTS1-F139 and $G_{\alpha i1}$-F336 simply do not interact, in contrast to the interaction seen for β2AR-F175 and $G\alpha_s$-F376. However, it is also possible that the phenylalanines do interact, and mutation of $G_{\alpha i1}$-F336 to an alanine is not severe enough to ablate binding. Indeed, if, as for β2AR-F175, a hydrophobic pocket on the G protein surrounds NTS1-F139 (figure 4), then an alanine may well be able to make hydrophobic interactions that compensate sufficiently for the lost phenylalanine-phenylalanine interaction.

4.2.C) Effect of lipid environment

Previous SPR results for the NTS1-$G\alpha_{i1}$ interaction described in section 1.5.B were obtained in POPC-POPG nanodiscs in the presence of NT_{8-13}. Unusual response profiles (figure 23) for the equivalent conditions conducted in BPL-nanodiscs limit the quantitative analysis of these results, but it seems likely that the interactions being studied are of an affinity at least as high as those observed in POPC-POPG nanodiscs. The results in section 3.4.B suggest an interaction in the system is saturated or approaches saturation after injection of analyte at 31nM. Support for this argument comes from experiments at lower analyte concentration (figure 24). Additionally, the fact that the NTS1-$G\alpha_{i1}$ interaction in the presence of SR48692 is weaker (figure 25) and does not show the unusual response profile seen in figure 23 supports this argument. Hence it seems likely that the NTS1-$G\alpha_{i1}$ interactions in BPL nanodiscs (in the presence and absence of NT_{8-13}) have a K_D<<30nM, especially since the analyte sample used may also contain empty nanodiscs. This is consistent with results from the host laboratory using microscale-thermophoresis that show the NTS1-$G\alpha_{i1}$ interaction to have highest affinity in a BPL environment (P. Dijkman & A. Watts, in preparation).

4.2.D) Future experiments

The most pressing experiments for the immediate future are repeats of the experiments described in order to assess the reproducibility of the system and gauge error. For the NT-bound and Apo states of the receptor, experiments using an analyte concentration range of 13-200nM should eliminate the unusual response profile seen in figure 23, and so allow for valid kinetic analysis.

In addition, the SPR results were limited by heterogeneity in the analyte and ligand, and by the lack of suitable conditions for the regeneration of the chip surface. The latter factor also severely limited the number of experiments possible. A homogeneous orientation of G protein on the chip surface could be achieved by site-specific biotinylation of the protein and use of a capture system such as the biotin CAPture kit (Biacore) (figure 26). This system also allows for easy regeneration of the chip surface. Heterogeneity in the analyte might be eliminated by inclusion of an additional nanodisc purification step; in particular, sucrose density-gradient ultracentrifugation has been successfully used to separate empty nanodiscs from those loaded with monomeric or dimeric SecY (Dalal *et al*, 2012).

Once such improvements have been implemented, in the longer term constructs with different mutations of the $G_{\alpha i1}$-F336 residue could be designed, expressed and assayed to further dissect the NTS1- $G\alpha_{i1}$ interface. Two possible mutations are suggested in table 11.

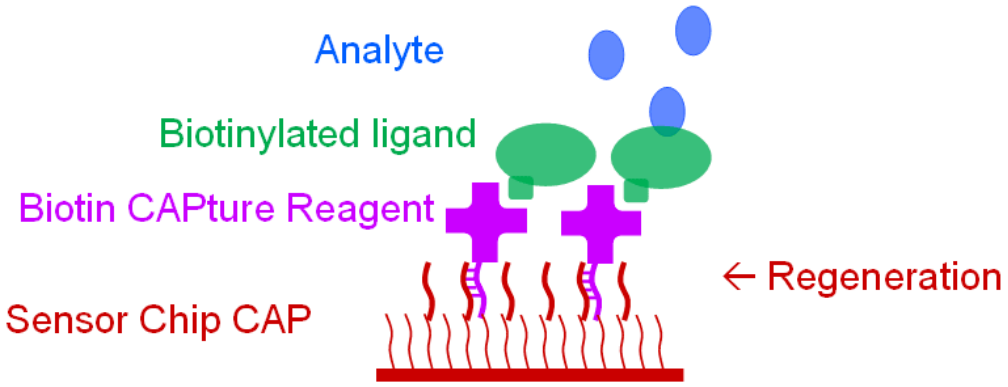

Figure 26: The Biotin CAPture Kit system (Biacore). This system involves capture of biotinylated ligand by a reagent that is coupled to the chip surface by a base pairing interaction. This interaction can be disrupted under defined conditions to regenerate the chip surface. Figure reproduced from that published on the Biacore website at the following address: https://www.biacore.com/lifesciences/products/Consumables/featured_consumables/biotin_CAPture_kit/index.html

$G\alpha_{i1}$ mutation	Rationale
F336S	Serine has a small side chain like alanine, but the polarity introduced by the –OH group may help to probe for the existence of hydrophobic interactions at the NTS1-Gai1 interface; if these interactions exist then serine is likely to perturb them more than alanine (provided the F336S protein can be expressed in a folded form).
F336Y	Tyrosine spatially mimics phenylalanine closely, but like serine would introduce polarity to the local environment.

Table 11: Possible future $G\alpha_{i1}$ F336 mutations to test.

An additional long-term aim would be to assay the interaction between NTS1-nanodiscs and the entire G protein heterotrimer; whilst the beta and gamma subunits make no direct contacts with the GPCR, they still influence the interaction of Gα with the GPCR (Chung *et al*, 2011).

5. BIBLIOGRAPHY

Adamson RJ & Watts A (2014) Kinetics of the early events of GPCR signalling. *FEBS Lett.* **588:** 4701–4707

Alves ID, Salamon Z, Varga E, Yamamura HI, Tollin G & Hruby VJ (2003) Direct observation of G-protein binding to the human delta-opioid receptor using plasmon-waveguide resonance spectroscopy. *J. Biol. Chem.* **278:** 48890–48897

Attrill H, Harding PJ, Smith E, Ross S & Watts A (2009) Improved yield of a ligand-binding GPCR expressed in E. coli for structural studies. *Protein Expr. Purif.* **64:** 32–38

Barroso S, Richard F, Nicolas-Ethève D, Kitabgi P & Labbé-Jullié C (2002) Constitutive activation of the neurotensin receptor 1 by mutation of Phe(358) in Helix seven. *Br. J. Pharmacol.* **135:** 997–1002

Bartfai T, Benovic JL, Bond RA, Bouvier M, Civelli O, Devi LA, George SR, Inui A, Kobilka B, Leurs R, Neubig R, Pin J, Roques BP & Seifert R (2004) The state of GPCR research in 2004. *Nat. Rev. Drug Discov.* **3:** 575, 577–626

Bayburt TH & Sligar SG (2010) Membrane protein assembly into Nanodiscs. *FEBS Lett.* **584:** 1721–1727

Bernaudat F, Frelet-Barrand A, Pochon N, Dementin S, Hivin P, Boutigny S, Rioux JB, Salvi D, Seigneurin-Berny D, Richaud P, Joyard J, Pignol D, Sabaty M, Desnos T, Pebay-Peyroula E, Darrouzet E, Vernet T & Rolland N (2011) Heterologous expression of membrane proteins: Choosing the appropriate host. *PLoS One* **6:** e29191

Borch J, Torta F, Sligar SG & Roepstorff P (2008) Nanodiscs for immobilization of lipid bilayers and membrane receptors: Kinetic analysis of cholera toxin binding to a glycolipid receptor. *Anal. Chem.* **80:** 6245–6252

Brzostowski J a. & Kimmel AR (2001) Signaling at zero G: G-protein-independent functions for 7-TM receptors. *Trends Biochem. Sci.* **26:** 291–297

Chung KY, Rasmussen SGF, Liu T, Li S, DeVree BT, Chae PS, Calinski D, Kobilka BK, Woods VL & Sunahara RK (2011) Conformational changes in the G protein Gs induced by the β2 adrenergic receptor. *Nature* **477:** 611–615

Civjan NR, Bayburt TH, Schuler MA & Sligar SG (2003) Direct solubilization of heterologously expressed membrane proteins by incorporation into nanoscale lipid bilayers. *Biotechniques* **35:** 556–563

Dalal K, Chan CS, Sligar SG & Duong F (2012) Two copies of the SecY channel and acidic lipids are necessary to activate the SecA translocation ATPase. *Proc. Natl. Acad. Sci.* **109:** 4104–4109

Davies MN, Secker A, Freitas A a., Mendao M, Timmis J & Flower DR (2007) On the hierarchical classification of G protein-coupled receptors. *Bioinformatics* **23:** 3113–3118

Denisov IG, Grinkova Y V, Lazarides AA, Sligar SG, Science M, V DU & Carolina N (2004) Directed Self-Assembly of Monodisperse Phospholipid Bilayer Nanodiscs with Controlled Size. *J. Am. Chem. Soc.* **126:** 3477–3487

Dobner PR (2005) Multitasking with neurotensin in the central nervous system. *Cell. Mol. Life Sci.* **62:** 1946–1963

Dorsam RT & Gutkind JS (2007) G-protein-coupled receptors and cancer. *Nat. Rev. Cancer* **7:** 79–94

Drescher DG, Ramakrishnan NA & Drescher MJ (2009) Surface Plasmon Resonance (SPR) Analysis of Binding Interactions of Proteins in Inner-Ear Sensory Epithelia Dennis. In *Methods in molecular biology,* Clifton, N.J. *(ed)* pp 323–343.

Egloff P, Deluigi M, Heine P, Balada S & Plückthun A (2014a) A cleavable ligand column for the rapid isolation of large quantities of homogeneous and functional neurotensin receptor 1 variants from E. coli. *Protein Expr. Purif.* **108:** 106–114

Egloff P, Hillenbrand M, Klenk C, Batyuk A, Heine P, Balada S, Schlinkmann KM, Scott DJ, Schütz M & Plückthun A (2014b) Structure of signaling-competent

neurotensin receptor 1 obtained by directed evolution in *Escherichia coli*. *Proc. Natl. Acad. Sci.* **111:** E655–62

Fredriksson R, Lagerström MC, Lundin L-G & Schiöth HB (2003) The G-protein-coupled receptors in the human genome form five main families. Phylogenetic analysis, paralogon groups, and fingerprints. *Mol. Pharmacol.* **63:** 1256–1272

George SR, O'Dowd BF & Lee SP (2002) G-protein-coupled receptor oligomerization and its potential for drug discovery. *Nat. Rev. Drug Discov.* **1:** 808–820

Glück JM, Koenig BW & Willbold D (2011) Nanodiscs allow the use of integral membrane proteins as analytes in surface plasmon resonance studies. *Anal. Biochem.* **408:** 46–52

Greentree WK & Linder ME (2004) Purification of recombinant G protein alpha subunits from Escherichia coli. *Methods Mol. Biol.* **237:** 3–20

Grisshammer R, White JF, Trinh LB & Shiloach J (2005) Large-scale expression and purification of a G-protein-coupled receptor for structure determination -- an overview. *J Struct Funct Genomics* **6:** 159–163

Grisshammer R (2009) Purification of Recombinant G-Protein-Coupled Receptors. *Methods Enzymol.* **463:** 631–645

Harding PJ, Attrill H, Boehringer J, Ross S, Wadhams GH, Smith E, Armitage JP & Watts A (2009) Constitutive dimerization of the G-Protein coupled receptor, neurotensin receptor 1, reconstituted into phospholipid bilayers. *Biophys. J.* **96:** 964–973

Inagaki S, Ghirlando R, White JF, Gvozdenovic-Jeremic J, Northup JK & Grisshammer R (2012) Modulation of the interaction between neurotensin receptor NTS1 and Gq protein by lipid. *J. Mol. Biol.* **417:** 95–111

Jaakola V-P, Griffith M., Hanson M., Cherezov V, Chien EY., Lane J., Ijzerman A. & Stevens RC (2008) The 2.6 Angstrom Crystal Structure of a Human A2A Adenosine Receptor Bound to an Antagonist. *Science.* **322:** 1211–1217

Jason-Moller L, Murphy M & Bruno J (2006) Overview of Biacore systems and their applications. *Curr. Protoc. protein Sci.***:** 45:19.13.1–19.13.14

Jesorka A & Orwar O (2008) Liposomes: technologies and analytical applications. *Annu. Rev. Anal. Chem. (Palo Alto. Calif).* **1:** 801–832

Johnston C a., Lobanova ES, Shavkunov AS, Low J, Ramer JK, Blaesius R, Fredericks Z, Willard FS, Kuhlman B, Arshavsky VY & Siderovski DP (2006) Minimal determinants for binding activated Gα from the structure of a Gαil-peptide dimer. *Biochemistry* **45:** 11390–11400

Katritch V, Cherezov V & Stevens RC (2013) Structure-function of the G protein-coupled receptor superfamily. *Annu Rev Pharmacol Toxicol* **53:** 531–556

Kenakin T (2004) Efficacy as a vector: the relative prevalence and paucity of inverse agonism. *Mol. Pharmacol.* **65:** 2–11

Kenakin T (2009) Biased agonism. *F1000 Biol. Rep.* **1:** 87 (doi:10.3410/B1-87)

Kitabgi P (2006) Functional domains of the subtype 1 neurotensin receptor (NTS1). *Peptides* **27:** 2461–2468

Kitabgi P, Carraway R, Van Rietschoten J, Granier C, Morgat JL, Menez a, Leeman S & Freychet P (1977) Neurotensin: specific binding to synaptic membranes from rat brain. *Proc. Natl. Acad. Sci. U. S. A.* **74:** 1846–1850

Knepp AM, Grunbeck A, Banerjee S, Sakmar TP & Huber T (2011) Direct measurement of thermal stability of expressed CCR5 and stabilization by small molecule ligands. *Biochemistry* **50:** 502–511

Lagerström MC & Schiöth HB (2008) Structural diversity of G protein-coupled receptors and significance for drug discovery. *Nat. Rev. Drug Discov.* **7:** 339–357

Leitz AJ, Bayburt TH, Barnakov AN, Springer B a. & Sligar SG (2006) Functional reconstitution of beta-2-adrenergic receptors utilizing self-assembling Nanodisc technology. *Biotechniques* **40:** 601–612

Le Maire M, Champeil P & Møller J V. (2000) Interaction of membrane proteins and lipids with solubilizing detergents. *Biochim. Biophys. Acta - Biomembr.* **1508:** 86–111

Manglik A & Kobilka B (2014) The role of protein dynamics in GPCR function: Insights from the β2AR and rhodopsin. *Curr. Opin. Cell Biol.* **27:** 136–143

Marty MT, Wilcox KC, Klein WL & Sligar SG (2013) Nanodisc-solubilized membrane protein library reflects the membrane proteome. *Anal. Bioanal. Chem.* **405:** 4009–4016

McEwen DP, Gee KR, Kang HC & Neubig RR (2001) Fluorescent BODIPY-GTP analogs: real-time measurement of nucleotide binding to G proteins. *Anal. Biochem.* **291:** 109–117

Mitra N, Liu Y, Liu J, Serebryany E, Mooney V, Devree BT, Sunahara RK & Yan ECY (2013) Calcium-dependent ligand binding and g-protein signaling of family B GPCR parathyroid hormone 1 receptor purified in nanodiscs. *ACS Chem. Biol.* **8:** 617–625

Mustain WC, Rychahou PG & Evers BM (2011) The role of neurotensin in physiologic and pathologic processes. *Curr. Opin. Endocrinol. Diabetes. Obes.* **18:** 75–82

Oakley RH, Laporte S a., Holt J a., Barak LS & Caron MG (2001) Molecular Determinants Underlying the Formation of Stable Intracellular G Protein-coupled Receptor-β-Arrestin Complexes after Receptor Endocytosis. *J. Biol. Chem.* **276:** 19452–19460

Oates J, Faust B, Attrill H, Harding P, Orwick M & Watts a (2012) The role of cholesterol on the activity and stability of neurotensin receptor 1. *Biochim Biophys Acta* **1818:** 2228–2233

Patching SG (2014) Surface plasmon resonance spectroscopy for characterisation of membrane protein-ligand interactions and its potential for drug discovery. *Biochim. Biophys. Acta* **1838:** 43–55

Pelaprat D (2006) Interactions between neurotensin receptors and G proteins. *Peptides* **27:** 2476–2487

Pierce KL, Premont RT & Lefkowitz RJ (2002) Seven-transmembrane receptors. *Nat. Rev. Mol. Cell Biol.* **3:** 639–650

Rask-Andersen M, Almén MS & Schiöth HB (2011) Trends in the exploitation of novel drug targets. *Nat. Rev. Drug Discov.* **10:** 579–590

Rasmussen SGF, DeVree BT, Zou Y, Kruse AC, Chung KY, Kobilka TS, Thian FS, Chae PS, Pardon E, Calinski D, Mathiesen JM, Shah ST a., Lyons J a., Caffrey M, Gellman SH, Steyaert J, Skiniotis G, Weis WI, Sunahara RK & Kobilka BK (2011) Crystal structure of the β2 adrenergic receptor–Gs protein complex. *Nature* **477:** 549–555

Ritchie TK, Grinkova Y V, Bayburt TH, Denisov IG, Zolnerciks JK, Atkins WM & Sligar SG (2009) Chapter 11 Reconstitution of Membrane Proteins in Phospholipid Bilayer Nanodiscs. *Methods Enzymol.* **464:** 211–231

Serebryany E, Zhu GA & Yan ECY (2012) Artificial membrane-like environments for in vitro studies of purified G-protein coupled receptors. *Biochim. Biophys. Acta - Biomembr.* **1818:** 225–233

Stenlund P, Babcock GJ, Sodroski J & Myszka DG (2003) Capture and reconstitution of G protein-coupled receptors on a biosensor surface. *Anal. Biochem.* **316:** 243–250

Tucker J & Grisshammer R, (1996) Purification of a rat neurotensin receptor expressed in Escherichia coli. *Biochem. J.* **317:** 891–899

Vincent JP, Mazella J & Kitabgi P (1999) Neurotensin and Receptors. *Trends Pharmacol. Sci.* **20:** 302–309

Vita N, Laurent P, Lefort S, Chalon P, Dumont X, Kaghad M, Gully D, Le Fur G, Ferrara P & Caput D (1993) Cloning and expression of a complementary DNA encoding a high affinity human neurotensin receptor. *FEBS Lett.* **317:** 139–142

White JF & Grisshammer R (2010) Stability of the neurotensin receptor NTS1 free in detergent solution and immobilized to affinity resin. *PLoS One* **5:** e12579

White JF, Noinaj N, Shibata Y, Love J, Kloss B, Xu F, Gvozdenovic-Jeremic J, Shah P, Shiloach J, Tate CG, Grisshammer R & Neurotensin (2012) Structure of the agonist-bound neurotensin receptor. *Nature* **490:** 508–515

Wilson WD (2002) Analyzing Biomolecular Interactions. *Science.* **295:** 2103–2105